Direct Numerical Simulations of the Navier-Stokes Alpha Model

Shiyi Chen[1,2], Darryl D. Holm[1], Len G. Margolin[3] and Raoyang Zhang[1,4]

[1]Center for Nonlinear Studies and Theoretical Division, Los Alamos National Laboratory, Los Alamos, NM 87545

[2]IBM Research Division, T.J. Watson Research Center, P.O. Box 218, Yorktown Heights, NY 10598

[3]Applied Theoretical and Computational Physics Division, Los Alamos National Laboratory, Los Alamos, NM 87545

[4]Department of Mechanical Engineering,126 Spencer Laboratory, University of Delaware, Newark, DE 19716

arXiv:chao-dyn/9902015v1 18 Feb 1999

Abstract

We explore the utility of the recently proposed alpha equations in providing a subgrid model for fluid turbulence. Our principal results are comparisons of direct numerical simulations of fluid turbulence using several values of the parameter alpha, including the limiting case where the Navier-Stokes equations are recovered. Our studies show that the large scale features, including statistics and structures, are preserved by the alpha models, even at coarser resolutions where the fine scales are not fully resolved. We also describe the differences that appear in simulations. We provide a summary of the principal features of the alpha equations, and offer some explanation of the effectiveness of these equations used as a subgrid model for three-dimensional fluid turbulence.

I. INTRODUCTION

Holm et al. [1], [2] introduced the "alpha models" for the mean motion of ideal incompressible fluids as the n-dimensional generalization of the one-dimensional Camassa-Holm (CH) equation. The 1D CH equation describes shallow water waves with nonlinear dispersion and admits soliton solutions called "peakons" [3]. Its n-dimensional generalization describes the slow time dynamics of fluids in which nonlinear dispersion accounts for the effects of the small scale rapid variability upon the mean motion. The fluid transport velocity is found by inversion of a Helmholtz operator acting on fluid circulation (or momentum) velocity. This operator contains a length scale that corresponds to the magnitude of the fluctuation covariance; the application of this operator smoothes the transport velocity relative to the circulation velocity. This length scale is denoted by α in references [1], [2], [3], hence the name *alpha models* for these mean fluid motion theories. The alpha models for self consistent mean fluid dynamics are derived by applying temporal averaging procedures to Hamilton's principle for an ideal incompressible fluid flow. The resulting mean fluid motion equations are obtained by using the Euler-Poincaré variational framework [1], [2]. (Euler-Poincaré equations are the Lagrangian version of Lie-Poisson Hamiltonian systems.) Therefore, these equations possess conservation laws for energy and momentum, as well as a Kelvin-Noether circulation theorem that establishes how the time average (or perhaps statistical) properties of the fluctuations affect the circulation of the mean flow. These ideal fluid equations also describe geodesic motion on the volume-preserving diffeomorphism group for a metric containing the H^1 norm of the mean fluid velocity. Their geometrical properties are discussed in [4]. Their relation to Eulerian and Lagrangian mean fluid theories is discussed in [5]. In recognition of their origins, these mean fluid motion equations may be known equally well by either the name alpha models, or CH equations.

Chen *et al.* [6] – [8] introduced phenomenological viscosity into the CH equation and proposed the resulting viscous Camassa-Holm equation (VCHE) as a closure approximation for the Reynolds averaged equations of the incompressible Navier-Stokes fluid. They

tested this approximation on turbulent channel and pipe flows with steady mean, by finding analytical solutions of the VCHE for the mean velocity and the Reynolds shear stress and comparing them with experiments [9]. They found that the steady VCHE profiles are consistent with data obtained from mean flow turbulence measurements in most of the flow region for channels and pipes at moderate to high Reynolds numbers. Thus, Chen *et al.* demonstrated a connection between turbulence and the VCHE for steady, or mean solutions. In fact, the *time-dependent* VCHE in a periodic box has unique classical solutions and a global attractor whose fractal dimension is finite and scales according to Kolmogorov's estimate, $N \sim (L/\ell_d)^3$, where $\ell_d = (\nu^3/\epsilon)^{1/4}$ is the Kolmogorov dissipation length [10]. We note that the time-dependent VCHE model is *not* equivalent to the Navier-Stokes equations with hyperviscosity, see [6] – [8], [10]. The VCHE model is also known as the Navier-Stokes alpha model, or the viscous alpha model.

The purpose of this paper is to compare the statistics and structures of the velocity and vorticity fields at moderate Reynolds numbers in a direct numerical simulation (DNS) of the viscous alpha model with the corresponding results for the Navier-Stokes equations. Through this comparison, we hope to determine whether the Navier-Stokes alpha model can be used as a subgrid model for fluid turbulence. The paper is arranged as follows: the mathematical background of the viscous alpha model and its connections with the Navier-Stokes equations are given in the next section. The remainder of the paper compares the classical Navier-Stokes DNS turbulence results with those for the viscous alpha models. In Section III we present the numerical methodology and energy spectra. Stretching dynamics, including the vorticity structure and the alignment phenomena are presented in Section IV. In Section V we present various two-point statistics, including the probability density function (PDF) of the velocity increment and the velocity structure functions. Concluding remarks are given in Section VI.

II. EULERIAN MEAN THEORY AND ALPHA MODEL EQUATIONS

Holm, Marsden, and Ratiu [1], [2] used variational asymptotics to obtain evolution equations for the Eulerian mean hydrodynamic motion of ideal incompressible fluids, employing an approximation of Hamilton's principle for Euler's equation in a Euclidean space setting. The method assumes that the Euler flow may be decomposed into its mean and fluctuating components at a fixed position in space. In their approach, a first-order Taylor expansion in the fluctuation amplitude is used to approximate the velocity field with the result that the L^2 metric in the Hamilton's principle giving rise to the Euler equations is replaced by an H^1 metric that produces the evolution equation of the Eulerian mean flow. We shall call this evolution equation the Euler alpha model, or the n-dimensional CH equation.

Holm et al. [4] give a geometrically intrinsic (i.e., coordinate free) derivation of these averaged equations by the procedure of *variational asymptotics*, namely, by deriving an averaged Lagrangian and using this Lagrangian to generate the equations via Hamilton's principle. This intrinsic setting is useful because many interesting flows, e.g., flows on spheres such as those in geophysics, do occur on manifolds. The standard decomposition into mean and fluctuating components is an additive decomposition, only valid in the presence of a vector space structure. We follow Holm [5] in presenting the derivation in Euclidean space.

We develop the Euler-Poincaré theory of advected fluctuations from the viewpoint of Eulerian averaging. Our point of departure is a Lagrangian comprised of the fluid kinetic energy in the Eulerian description, in which volume preservation is imposed by a Lagrange multiplier P (the pressure),

$$L(\omega) = \int d^3x \left\{ \frac{D}{2} |\mathbf{U}(\mathbf{x}, t\,; \omega)|^2 + P(\mathbf{x}, t\,; \omega) \Big(1 - D(\mathbf{x}, t\,; \omega) \Big) \right\} , \tag{1}$$

where D is the Eulerian volume element. We assume that there are two time scales for the motion: the fast time ω and the slow time t. The traditional Reynolds decomposition of fluid velocity into its fast and slow components is expressed at a given position $\mathbf{x}$ in terms

of the Eulerian mean fluid velocity $\mathbf{u}$ as

$$\mathbf{U}(\mathbf{x},t\,;\omega) \equiv \mathbf{u}(\mathbf{x},t) + \mathbf{u}'(\mathbf{x},t\,;\omega)\,. \tag{2}$$

Following Holm [5], we assume the Eulerian velocity fluctuation $\mathbf{u}'(\mathbf{x},t\,;\omega)$ is related to an Eulerian fluid parcel displacement fluctuation — denoted as $\boldsymbol{\zeta}(\mathbf{x},t\,;\omega)$ — by

$$\frac{\partial \boldsymbol{\zeta}}{\partial t} + \mathbf{u}\cdot\boldsymbol{\nabla}\boldsymbol{\zeta} = \boldsymbol{\zeta}\cdot\boldsymbol{\nabla}\mathbf{u} + \mathbf{u}'(\mathbf{x},t\,;\omega)\,. \tag{3}$$

For purely Eulerian velocity fluctuations as in Eq. (2), this relation separates into two relations: the "Taylor-like" hypothesis of [4],

$$\frac{\partial \boldsymbol{\zeta}}{\partial t} + \mathbf{u}\cdot\boldsymbol{\nabla}\boldsymbol{\zeta} = 0\,; \tag{4}$$

and the relation [4], [5]

$$0 = \boldsymbol{\zeta}\cdot\boldsymbol{\nabla}\mathbf{u} + \mathbf{u}'(\mathbf{x},t\,;\omega)\,. \tag{5}$$

Hence, the Reynolds velocity decomposition (2) separates the Lagrangian (1) into its mean and fluctuating pieces as

$$L(\omega) = \int d^3x \left\{ \frac{D}{2}\big|\mathbf{u}(\mathbf{x},t) + \mathbf{u}'(\mathbf{x},t\,;\omega)\big|^2 + P(\mathbf{x},t)\Big(1 - D(\mathbf{x},t)\Big)\right\}. \tag{6}$$

No modification is needed in the pressure constraint in this Lagrangian, because the Eulerian mean *preserves* the condition that the velocity be divergence free; hence, $\boldsymbol{\nabla}\cdot\mathbf{u} = 0$. It remains only to take the Eulerian mean of this Lagrangian, in which we assume $\langle\,\boldsymbol{\zeta}\,\rangle = 0$. The Eulerian mean averaging process at fixed position $\mathbf{x}$ is denoted $\langle\,\cdot\,\rangle$ with, e.g.,

$$\mathbf{u}(\mathbf{x},t) = \langle \mathbf{U}(\mathbf{x},t\,;\omega)\rangle \equiv \lim_{T\to\infty}\frac{1}{T}\int_0^T \mathbf{U}(\mathbf{x},t\,;\omega)\,d\omega\,. \tag{7}$$

By Eq. (5), the Eulerian mean kinetic energy due to the velocity fluctuation satisfies

$$\langle\,|\mathbf{u}'|^2\,\rangle = \langle \zeta^k\zeta^l\rangle \mathbf{u}_{,k}\cdot\mathbf{u}_{,l}\,. \tag{8}$$

Thus, we find the following Eulerian mean Lagrangian,

$$\langle L\rangle = \int d^3x \left\{ \frac{D}{2}\Big[\big|\mathbf{u}(\mathbf{x},t)\big|^2 + \langle\,\zeta^k\zeta^l\rangle \mathbf{u}_{,k}\cdot\mathbf{u}_{,l}\Big] + P(\mathbf{x},t)\Big(1 - D(\mathbf{x},t)\Big)\right\}. \tag{9}$$

The advection relation (4) implies the same advective velocity for each component of the symmetric Eulerian mean covariance tensor $\langle\,\zeta^k\zeta^l\rangle$. Thus, we have

$$\Big(\frac{\partial}{\partial t}+\mathbf{u}\cdot\boldsymbol{\nabla}\Big)\langle\,\zeta^k\zeta^l\rangle=0\,. \tag{10}$$

Together, this relation and the continuity equation for the volume element D,

$$\frac{\partial D}{\partial t}+\boldsymbol{\nabla}\cdot D\mathbf{u}=0\,, \tag{11}$$

complete the auxiliary equations needed for deriving the equation of motion for the Eulerian mean velocity $\mathbf{u}$ from the averaged Lagrangian $\langle L\rangle$ in (6) by using the Euler-Poincaré theory.

The results of [1] allow one to compute the Euler-Poincaré equation for the Lagrangian $\langle L\rangle$ in (6) depending on the Eulerian mean velocity $\mathbf{u}$, and the advected quantities D and $\langle\zeta^k\zeta^l\rangle$ as

$$\begin{aligned}0=\left(\frac{\partial}{\partial t}+u^j\frac{\partial}{\partial x^j}\right)\frac{1}{D}\frac{\delta\langle L\rangle}{\delta u^i}+\frac{1}{D}\frac{\delta\langle L\rangle}{\delta u^j}u^j_{,i}\\ -\frac{\partial}{\partial x^i}\frac{\delta\langle L\rangle}{\delta D}\;+\;\frac{1}{D}\frac{\delta\langle L\rangle}{\delta\langle\zeta^k\zeta^l\rangle}\;\frac{\partial}{\partial x^i}\langle\zeta^k\zeta^l\rangle\,.\end{aligned} \tag{12}$$

We compute the following variational derivatives of the averaged approximate Lagrangian $\langle L\rangle$ in Eq. (6)

$$\begin{aligned}\frac{1}{D}\frac{\delta\langle L\rangle}{\delta\mathbf{u}}&=\mathbf{u}-\frac{1}{D}\Big(\partial_k\,D\langle\zeta^k\zeta^l\rangle\partial_l\Big)\mathbf{u}\equiv\mathbf{v},\\ \frac{\delta\langle L\rangle}{\delta D}&=-P+\frac{1}{2}|\mathbf{u}\,|^2+\frac{1}{2}\langle\zeta^k\zeta^l\rangle\big(\mathbf{u}_{,k}\cdot\mathbf{u}_{,l}\big)\equiv-P_{tot},\\ \frac{\delta\langle L\rangle}{\delta P}&=1-D\,,\\ \frac{\delta\langle L\rangle}{\delta\langle\zeta^k\zeta^l\rangle}&=\frac{D}{2}\big(\mathbf{u}_{,k}\cdot\mathbf{u}_{,l}\big)\,.\end{aligned} \tag{13}$$

The Euler-Poincaré Eq. (12) for this averaged Lagrangian takes the form,

$$\frac{\partial\mathbf{v}}{\partial t}+\mathbf{u}\cdot\boldsymbol{\nabla}\,\mathbf{v}+v_j\boldsymbol{\nabla}\,u^j+\boldsymbol{\nabla}\,P_{tot}=-\,\frac{1}{2}\,\big(\mathbf{u}_{,k}\cdot\mathbf{u}_{,l}\big)\boldsymbol{\nabla}\,\langle\zeta^k\zeta^l\rangle\,, \tag{14}$$

$$\text{where}\quad\mathbf{v}=\mathbf{u}-\tilde{\Delta}_D\mathbf{u}\quad\text{with}\quad\tilde{\Delta}_D\equiv\frac{1}{D}\big(\partial_k\,D\,\langle\zeta^k\zeta^l\rangle\partial_l\big)\quad\text{and}\quad\boldsymbol{\nabla}\cdot\mathbf{u}=0\,. \tag{15}$$

Its definition as a variational derivative indicates that $\mathbf{v}$ is a specific momentum in a certain sense dual to the velocity $\mathbf{u}$. For more discussion of physical interpretations of $\mathbf{u}$ and

$\mathbf{v}$, see [5]. The Euler-Poincaré equations (14) – (15) define the Eulerian mean motion (EMM) model. Incompressibility of the Eulerian mean velocity $\mathbf{u}$ follows from the continuity equation (11) and the constraint $\delta\langle L\rangle/\delta P = 0$. A natural set of boundary conditions is

$$\mathbf{v}\cdot\hat{\boldsymbol{n}} = 0\,, \quad \mathbf{u} = 0\,, \quad \text{and} \quad \hat{\boldsymbol{n}}\cdot\langle\boldsymbol{\xi}\boldsymbol{\xi}\rangle = 0, \quad \text{on a fixed boundary.} \tag{16}$$

Then, provided the Helmholtz operator $1 - \tilde{\Delta}_D$ for $D = 1$ may be inverted, the Eulerian mean pressure P may be obtained by solving an elliptic equation.

A. Reducing the EMM equation to the n-dimensional CH equation

When the Eulerian mean covariance is isotropic and homogeneous, so that $\langle\zeta^k\zeta^l\rangle = \alpha^2\delta^{kl}$ (for a constant length scale α, whose magnitude is set by the initial conditions for the Eulerian mean covariance) then the EMM equation (14) **reduces** to the n-dimensional Camassa-Holm equation introduced in [1], [2], namely,

$$\frac{\partial\mathbf{v}}{\partial t} + \mathbf{u}\cdot\boldsymbol{\nabla}\,\mathbf{v} + v_j\boldsymbol{\nabla}u^j + \boldsymbol{\nabla}\,P_{tot} = 0\,, \quad \boldsymbol{\nabla}\cdot\mathbf{u} = 0 = \boldsymbol{\nabla}\cdot\mathbf{v}\,, \tag{17}$$

$$\text{where} \quad \mathbf{v} = \mathbf{u} - \alpha^2\Delta\mathbf{u}\,, \quad P_{tot} = P - \frac{1}{2}|\mathbf{u}\,|^2 - \frac{\alpha^2}{2}|\nabla\mathbf{u}\,|^2\,. \tag{18}$$

This n-dimensional CH equation set is an invariant subsystem of the Euler-Poincaré system (14), with definition (15) and advection law (10), because the homogeneous isotropic initial condition $\langle\zeta^k\zeta^l\rangle = \alpha^2\delta^{kl}$ is invariant under the dynamics of equation (10). Hence, any of the formulae above remain valid if we set $\langle\zeta^k\zeta^l\rangle = \alpha^2\delta^{kl}$, with constant α.

Equations of the type (17) but with additional dissipative terms were considered previously in the theory of second grade fluids [11] and were treated recently in the mathematical literature [12], [13]. Second grade fluid models are derived from continuum mechanical principles of objectivity and material frame indifference, after which thermodynamic principles such as the Clausius-Duhem relation and stability of stationary equilibrium states are imposed to restrict the allowed values of the parameters in these models. In contrast, the CH equation (17) is derived here by applying asymptotic expansions, Eulerian means, and an assumption of isotropy of fluctuations in Hamilton's principle for an ideal incompressible fluid.

This derivation provides the interpretation of the length scale α as the typical amplitude of the rapid fluctuations whose Eulerian mean is taken in Hamilton's principle.

The n-dimensional CH equation (17) implies the conservation of energy $\frac{1}{2}\int d^3x\, \mathbf{u}\cdot\mathbf{v}$ and helicity $\frac{1}{2}\int d^3x\, \mathbf{v}\cdot \mathrm{curl}\mathbf{v}$. Its steady vortical flows include the analogs of the Beltrami flows $\mathrm{curl}\mathbf{v} = \lambda\mathbf{u}$. In the periodic case, we define $\mathbf{v_k}$ as the $\mathbf{k}$-th Fourier mode of the specific momentum $\mathbf{v} \equiv (1-\alpha^2\Delta)\mathbf{u}$; so that $\mathbf{v_k} \equiv (1+\alpha^2|\mathbf{k}|^2)\mathbf{u_k}$. Then Eq. (17) becomes [1], [2]

$$\Pi_\perp \left(\frac{d}{dt}\mathbf{v_k} - i \sum_{\mathbf{p}+\mathbf{n}=\mathbf{k}} \frac{\mathbf{v_p}}{1+\alpha^2|\mathbf{p}|^2} \times (\mathbf{n}\times\mathbf{v_n}) \right) = 0, \tag{19}$$

where $\Pi_\perp$ is the Leray projection onto Fourier modes transverse to $\mathbf{k}$ (this ensures incompressibility). Hence, the nonlinear coupling among the modes is suppressed by the denominator when $1+\alpha^2|\mathbf{p}|^2 \gg |\mathbf{n}|$.

An essential feature of the n-dimensional CH equation (17) is that its specific momentum $\mathbf{v}$ is transported by a velocity $\mathbf{u}$ that is smoothed, or filtered, by application of the inverse elliptic Helmholtz operator $(1-\alpha^2\Delta)$. The effect on length scales smaller than α is that steep gradients of the specific momentum $\mathbf{v}$ tend not to steepen much further, and that thin vortex tubes tend not to get much thinner as they are transported. Furthermore, as our present numerical simulations shall verify, the effect on length scales larger than α is negligible. Hence, the n-dimensional CH equation preserves the assumptions under which it is derived.

B. Physical interpretation of v as the Lagrangian mean velocity

The Stokes mean drift velocity is defined by [14],

$$\langle \mathbf{U} \rangle^S \equiv \langle \boldsymbol{\zeta}\cdot\boldsymbol{\nabla}\mathbf{u}' \rangle\,. \tag{20}$$

Hence, Eq. (5) implies

$$\langle \mathbf{U} \rangle^S = -\langle \boldsymbol{\zeta}\cdot\boldsymbol{\nabla}\boldsymbol{\zeta}\cdot\boldsymbol{\nabla}\rangle\mathbf{u} = -\tilde{\Delta}\mathbf{u} + o(|\boldsymbol{\zeta}|^2)\,, \tag{21}$$

where

$$\tilde{\Delta} \equiv \big(\partial_k \langle \zeta^k \zeta^l \rangle \partial_l\big) = \tilde{\Delta}_D\big|_{D=1}\,, \tag{22}$$

and we argue that $\boldsymbol{\nabla}\cdot\boldsymbol{\zeta} = o(|\boldsymbol{\zeta}|^2)$. Thus, we find that $\mathbf{v}$ satisfies, to order $o(|\boldsymbol{\zeta}|^2)$,

$$\mathbf{v} \equiv \mathbf{u} - \tilde{\Delta}\mathbf{u} = \mathbf{u} + \langle \mathbf{U} \rangle^S = \langle \mathbf{U} \rangle^L\,. \tag{23}$$

Therefore to this order, $\mathbf{v}$ in the EMM theory is the Lagrangian mean velocity.

C. Kelvin circulation theorem for EMM and CH equations

Being Euler–Poincaré, the Eulerian mean motion (EMM) equation (14) and its invariant reduced form the CH equation (17) for $\langle \zeta^k \zeta^l \rangle = \alpha^2 \delta^{kl}$ has a corresponding Kelvin-Noether circulation theorem,

$$\frac{d}{dt}\oint_{\gamma(\mathbf{u})} \mathbf{v}\cdot d\mathbf{x} = -\frac{1}{2}\int\int_{S(\mathbf{u})} \boldsymbol{\nabla}\big(\mathbf{u}_{,k}\cdot\mathbf{u}_{,l}\big)\times\boldsymbol{\nabla}\langle\zeta^k\zeta^l\rangle\cdot d\mathbf{S}\,, \tag{24}$$

for any closed curve $\gamma(\mathbf{u})$ that moves with the Eulerian mean fluid velocity $\mathbf{u}$ and surface $S(\mathbf{u})$ with boundary $\gamma(\mathbf{u})$. Thus in this Kelvin-Noether circulation theorem, the presence of spatial gradients in the Eulerian mean fluctuation covariance $\langle \zeta^k \zeta^l \rangle$ creates circulation of the Lagrangian mean velocity $\mathbf{v} = \mathbf{u} - \tilde{\Delta}\mathbf{u}$.

D. Vortex stretching equation for the Eulerian mean model

In three dimensions, the EMM equation (14) may be expressed in its equivalent "curl" form, as

$$\frac{\partial}{\partial t}\mathbf{v} - \mathbf{u}\times\Big(\boldsymbol{\nabla}\times\mathbf{v}\Big) + \boldsymbol{\nabla}\big(P_{tot} + \mathbf{u}\cdot\mathbf{v}\big) = -\frac{1}{2}\big(\mathbf{u}_{,k}\cdot\mathbf{u}_{,l}\big)\boldsymbol{\nabla}\langle\zeta^k\zeta^l\rangle\,, \quad \boldsymbol{\nabla}\cdot\mathbf{u} = 0\,. \tag{25}$$

The curl of this equation in turn yields an equation for transport and creation for the Lagrangian mean vorticity, $\mathbf{q} \equiv \operatorname{curl}\mathbf{v}$,

$$\frac{\partial \mathbf{q}}{\partial t} + \mathbf{u}\cdot\boldsymbol{\nabla}\mathbf{q} = \mathbf{q}\cdot\boldsymbol{\nabla}\mathbf{u} - \frac{1}{2}\boldsymbol{\nabla}\big(\mathbf{u}_{,k}\cdot\mathbf{u}_{,l}\big)\times\boldsymbol{\nabla}\langle\zeta^k\zeta^l\rangle\,, \quad \text{where} \quad \mathbf{q} \equiv \operatorname{curl}\mathbf{v}\,, \tag{26}$$

and we have used incompressibility of $\mathbf{u}$. Thus $\mathbf{u}$ is the transport velocity for the generalized vorticity $\mathbf{q}$, and the expected vortex stretching term $\mathbf{q}\cdot\boldsymbol{\nabla}\,\mathbf{u}$ is accompanied by an additional vortex creation term proportional to the Eulerian mean covariance gradient. Of course, this additional term is also responsible for the creation of circulation of $\mathbf{v}$ in the Kelvin-Noether circulation theorem (24) and vanishes when the Eulerian mean covariance is homogeneous in space, thereby recovering the corresponding result for the three dimensional CH equation [1], [2].

E. Energetics of the Eulerian mean model

Noether's theorem guarantees conservation of energy for the Euler-Poincaré equations (14), since the Eulerian mean Lagrangian $\langle L\rangle$ in Eq. (6) has no explicit dependence on time. This constant energy is given by

$$E_t = \frac{1}{2}\int d^3x \Big(|\mathbf{u}\,|^2 + \langle \zeta^k \zeta^l \rangle \mathbf{u}_{,k}\cdot\mathbf{u}_{,l}\Big) = \frac{1}{2}\int d^3x\ \mathbf{u}\cdot\mathbf{v}\,. \tag{27}$$

Thus, the total kinetic energy is the integrated product of the Eulerian mean and Lagrangian mean velocities. In this kinetic energy, the Eulerian mean covariance of the fluctuations couples to the gradients of the Eulerian mean velocity. So there is a cost in kinetic energy for the system either to increase these gradients, or to increase the Eulerian mean covariance.

F. Momentum conservation – stress tensor formulation

Noether's theorem also guarantees conservation of momentum for the Euler-Poincaré equation (14), since the Eulerian mean Lagrangian $\langle L\rangle$ in Eq. (6) has no explicit spatial dependence. In momentum conservation form, Eq. (14) becomes

$$\frac{\partial v_i}{\partial t} = -\,\frac{\partial}{\partial x^j}\Big(v_i\, u^j + P\delta_i^j - \mathbf{u}_{,k}\cdot\mathbf{u}_{,i}\,\langle \zeta^k\zeta^j\rangle\Big)\,. \tag{28}$$

The boundary conditions are given in Eq. (16).

G. A second moment turbulence closure model for EMM

When dissipation and forcing are added to the EMM motion equation (14) by using the phenomenological viscosity $\nu\tilde{\Delta}\mathbf{v}$ and forcing $\mathbf{F}$, one finds a **second moment Eulerian mean turbulence model** given by

$$\Big(\frac{\partial}{\partial t} + \mathbf{u}\cdot\boldsymbol{\nabla}\Big)\mathbf{v} + v_j\boldsymbol{\nabla}u^j + \boldsymbol{\nabla}P_{tot} + \frac{1}{2}\big(\mathbf{u}_{,k}\cdot\mathbf{u}_{,l}\big)\boldsymbol{\nabla}\langle\zeta^k\zeta^l\rangle = \nu\,\tilde{\Delta}\mathbf{v} + \mathbf{F}\,, \quad \text{where} \quad \boldsymbol{\nabla}\cdot\mathbf{u} = 0\,, \tag{29}$$

with viscous boundary conditions $\mathbf{v} = 0$, $\mathbf{u} = 0$ at a fixed boundary. Note that the Eulerian mean fluctuation covariance $\langle\zeta^k\zeta^j\rangle$ appears in the dissipation operator $\tilde{\Delta}$. In the absence of the forcing $\mathbf{F}$, this viscous EMM turbulence model dissipates the energy E in Eq. (27) according to

$$\frac{dE}{dt} = -\,\nu\int d^3x\Big[\mathrm{tr}(\boldsymbol{\nabla}\mathbf{u}^T\cdot\langle\boldsymbol{\zeta}\boldsymbol{\zeta}\rangle\cdot\boldsymbol{\nabla}\mathbf{u}) + \tilde{\Delta}\mathbf{u}\cdot\tilde{\Delta}\mathbf{u}\Big]\,. \tag{30}$$

This negative definite energy dissipation law is a consequence of adding viscosity with $\tilde{\Delta}$, instead of using the ordinary Laplacian operator. In the isotropic homogeneous case of this model, where $\langle\zeta^k\zeta^l\rangle = \alpha^2\delta^{kl}$ (for a constant length scale α) we find the viscous Camassa-Holm equation (VCHE), or the Navier-Stokes alpha model,

$$\Big(\frac{\partial}{\partial t} + \mathbf{u}\cdot\boldsymbol{\nabla}\Big)\mathbf{v} + v_j\boldsymbol{\nabla}u^j + \boldsymbol{\nabla}P_{tot} = \nu\alpha^2\,\Delta\mathbf{v} + \mathbf{F}\,, \quad \text{where} \quad \boldsymbol{\nabla}\cdot\mathbf{u} = 0\,, \tag{31}$$

where Δ is the usual Laplacian operator for this case and $\mathbf{v}$ and P_{tot} are defined in (18).

H. Constitutive interpretation of the VCHE

Chen et al. [6]– [8] gave a continuum mechanical interpretation to the VCHE closure model, by rewriting the VCHE (31) in the equivalent **constitutive form**,

$$\frac{d\mathbf{u}}{dt} = \mathrm{div}\mathbf{T}\ ,\ \mathbf{T} = -p\mathbf{I} + 2\nu(1-\alpha^2\Delta)\mathbf{D} + 2\alpha^2\dot{\mathbf{D}}\ , \tag{32}$$

with $\boldsymbol{\nabla}\cdot\mathbf{u} = 0, \mathbf{D} = (1/2)(\boldsymbol{\nabla}\mathbf{u}+\boldsymbol{\nabla}\mathbf{u}^T)$, $\boldsymbol{\Omega} = (1/2)(\boldsymbol{\nabla}\mathbf{u}-\boldsymbol{\nabla}\mathbf{u}^T)$, and co-rotational (Jaumann) derivative given by $\dot{\mathbf{D}} = d\mathbf{D}/dt + \mathbf{D}\,\boldsymbol{\Omega} - \boldsymbol{\Omega}\mathbf{D}$, with $d/dt = \partial/\partial t + \mathbf{u}\cdot\boldsymbol{\nabla}$. In this form, one

recognizes the constitutive form of VCHE as a variant of the rate-dependent incompressible homogeneous fluid of second grade [15], [16], whose viscous dissipation, however, is *modified* by the Helmholtz operator $(1-\alpha^2\Delta)$. There is a tradition at least since Rivlin [17] of modeling turbulence by using continuum mechanics principles such as objectivity and material frame indifference (see also [18]). For example, this sort of approach is taken in deriving Reynolds stress algebraic equation models [19]. Rate-dependent closure models of mean turbulence such as the VCHE have also been obtained by a two-scale DIA approach [20] and by renormalization group methods [21].

I. Comparison of VCHE with LES and RANS models

Reynolds-averaged Navier-Stokes (RANS) models of turbulence are part of the classic theoretical development of the subject [22], [23], [24]. The related Large Eddy Simulation (LES) turbulence modeling approach [25], [26], [27], provides an operational definition of the intuitive idea of Eulerian resolved scales of motion in turbulent flow. In this approach a filtering function $\mathcal{F}(\mathbf{r})$ is introduced and the Eulerian velocity field $\mathbf{U}_E$ is filtered in an integral sense, as

$$\bar{\mathbf{u}}(\mathbf{r}) \equiv \int_{R^3} d^3r' \; \mathcal{F}(\mathbf{r}-\mathbf{r}')\,\mathbf{U}_E\,(\mathbf{r}')\,. \tag{33}$$

This convolution of $\mathbf{U}_E$ with $\mathcal{F}$ defines the large scale, resolved, or filtered velocity, $\bar{\mathbf{u}}$. The corresponding small scale, or subgrid scale velocity, $\mathbf{u}'$, is then defined as the difference,

$$\mathbf{u}'(\mathbf{r}) \equiv \mathbf{U}_E\,(\mathbf{r}) - \bar{\mathbf{u}}\,(\mathbf{r})\,. \tag{34}$$

When this filtering operation is applied to the Navier-Stokes system, the following dynamical equation is obtained for the filtered velocity, $\bar{\mathbf{u}}$, cf. Eq. (32),

$$\frac{\partial}{\partial t}\bar{\mathbf{u}} + \bar{\mathbf{u}}\cdot\boldsymbol{\nabla}\,\bar{\mathbf{u}} = -\,\mathrm{div}\overline{\mathbf{T}} - \,\boldsymbol{\nabla}\bar{p} + \nu\,\Delta\bar{\mathbf{u}}\,, \quad \boldsymbol{\nabla}\cdot\bar{\mathbf{u}} = 0\,, \tag{35}$$

in which $\bar{p}$ is the filtered pressure field (required to maintain $\boldsymbol{\nabla} \cdot \bar{\mathbf{u}} = 0$) and the tensor difference

$$\overline{\mathbf{T}} = \overline{(\mathbf{U}_E \mathbf{U}_E)} - \bar{\mathbf{u}}\bar{\mathbf{u}}\,, \tag{36}$$

represents the subgrid scale stress due to the turbulent eddies. This subgrid scale stress tensor appears in the same form as the Reynolds stress tensor obtained from Reynolds averaging the Navier-Stokes equation.

The results of Chen et al. [6]– [8], may be given either an LES, or RANS interpretation simply by comparing the constitutive form of the VCHE in (32) term by term with equation (35), provided one may ignore the difference between Eulerian mean, and Lagrangian mean velocities as being of higher order. Additional LES interpretations, discussions and numerical results for forced-turbulence simulations of the VCHE model, or the Navier-Stokes alpha model, will be presented below.

III. DIRECT NUMERICAL SIMULATION, RELATED DEFINITIONS AND ENERGY SPECTRA

In Fourier space, the viscous alpha model equation (25) with isotropic viscosity can be written for the Lagrangian mean velocity $\mathbf{v}$ as follows:

$$\frac{\partial \mathbf{v}_\mathbf{k}}{\partial t} = \hat{P}(\mathbf{k})(\mathbf{u} \times \mathbf{q})_\mathbf{k} - \nu k^2 \mathbf{v}_\mathbf{k} + \mathbf{f}_\mathbf{k}, \tag{37}$$

$$\mathbf{k} \cdot \mathbf{v}_\mathbf{k} = 0, \tag{38}$$

where $\hat{P}_{ij} = \delta_{ij} - k_i k_j / k^2$ is the incompressible projection operator. The Eulerian mean velocity satisfies $\mathbf{u} = (1 - \alpha^2 \Delta)^{-1} \mathbf{v}$ (or $\mathbf{u}(\mathbf{k}) = (1 + \alpha^2 k^2)^{-1} \mathbf{v}(\mathbf{k})$), $\mathbf{q} = \nabla \times \mathbf{v}$ and $\mathbf{f}_\mathbf{k}$ is the forcing term for the $\mathbf{k}$-th velocity component. We emphasize that $1/\alpha$ acts as the cutoff wavenumber for the nonlinearity in alpha model.

A pseudo-spectral code has been developed for solving the above equations in a cubic box for periodic boundary conditions. The code is written in message-passing language for the SGI-ORIGIN-2000 machine in the Advanced Computing Laboratory at the Los Alamos National Laboratory. The viscous term is integrated analytically in time. The other terms are discretized using a second-order Adams-Bashforth scheme. The nonlinear terms are calculated using pseudo-spectral methods [28]. The time evolution of Eq. (37) can be written:

$$\frac{\mathbf{v}_{\mathbf{k}}^{n+1} - \mathbf{v}_{\mathbf{k}}^{n} exp(-\nu k^2 \Delta t)}{\Delta t} = \hat{P}(\mathbf{k})[\frac{3}{2}(\mathbf{u} \times \mathbf{q})_{\mathbf{k}}^{n} exp(-\nu k^2 \Delta t) - \frac{1}{2}(\mathbf{v} \times \mathbf{q})_{\mathbf{k}}^{n-1} exp(-2\nu k^2 \Delta t)] + f_{\mathbf{k}}. \quad (39)$$

In this paper, we adopt the following definitions: the mean velocity fluctuation, u', is defined as

$$u' = \sqrt{\frac{2}{3} E_t} = (\frac{2}{3} \int_o^\infty E(k) dk)^{\frac{1}{2}};$$

where E_t is the total energy defined in Eq. (27) and $E(k)$ is the energy spectrum:

$$E(k) = \sum_{\mathbf{k}-1/2}^{\mathbf{k}+1/2} \mathbf{u}(\mathbf{k}') \cdot \mathbf{v}(\mathbf{k}').$$

The Taylor microscale and the mean dissipation rate are defined respectively as follows:

$$\lambda = (15\nu/\epsilon)^{1/2} u',$$

$$\epsilon = 2\nu \int_o^\infty k^2 E(k) dk.$$

The large eddy turn-over time is given by:

$$\tau = \frac{L_f}{u'}.$$

where L_f is the integral length. The Kolmogorov dissipation scale η is defined as $(\nu^3/\epsilon)^{\frac{1}{4}}$, with corresponding wave number $k_d = 1/\eta$. The Taylor microscale Reynolds number is defined by

$$R_\lambda = \frac{u'\lambda}{\nu}.$$

To maintain a statistical steady state, the forcing term $\mathbf{f_k}$ was introduced in the first two shells of the Fourier modes ($k < 2.5$), in which the kinetic energy of each mode in the two shells was forced to be constant in time, while the energy ratio between shells consistent with $k^{-5/3}$ in order to approximate a larger inertial sub-range [28]. Most simulations were carried out for about ten large eddy turnover times before recording any data. The initial velocity was a Gaussian field with a prescribed energy spectrum: $\sim k^4 exp[-(k/k_0)^2]$, where k_0 is a constant whose value is approximately 5. Statistics were obtained by averaging physical quantities over several eddy turnover times.

DNS has been carried out for three cases: with $\alpha = 0$ (the Navier-Stokes equations), $1/32$ and $1/8$ for the same viscosity $\nu = 0.001$. The corresponding R_λ are $147, 182$ and 279, respectively. In Fig. 1, we show the energy spectra of the three simulations. We note that because each simulation used the same viscosity, the higher Reynolds number flows correspond to smaller Taylor microscales, leading to more compact energy spectra. This is similar to the results of subgrid simulations for higher Reynolds number flows [29]. In Fig. 2, we compare the energy spectrum for $\alpha = 1/8$ with mesh sizes of 256^3 and 64^3. It is seen that the energy spectrum at the large scales (in the inertial range) are the same, indicating that the large scale flow properties for $\alpha = 1/8$ can be preserved in a less-resolved simulation.

To see how the energy cascades from the large scale modes to the small scale modes, in Fig. 3 we show the energy transfer spectrum,

$$\Pi(k) \equiv \mathbf{v}(\mathbf{k}) \cdot \hat{P}(\mathbf{k})(\mathbf{u} \times \mathbf{q})_\mathbf{k},$$

as a function of the wave number, k. We note that the energy transfer spectrum for all three cases with different α's are constant and agree quite well in the inertial range for $k < 20$, except for the effect of noise. This result indicates that the alpha model preserves the fundamental properties of the Kolmogorov energy cascade in the inertial range [29]. For the dissipation range ($k > 20$), however, the change of the energy transfer spectrum is significant for $\alpha = 1/8$.

IV. VORTICITY STRUCTURES AND ALIGNMENT

As contrasted with the hyperviscosity approach [30,31] in which the normal dissipation operator is replaced by a higher order Laplace operator and therefore only small scale fluid motions are affected, in the alpha model the nonlinear vortex stretching dynamics is modified as shown in Eq. (26), where the vorticity $\mathbf{q}$ is defined by the curl of the velocity $\mathbf{v}$ while the advective velocity is $\mathbf{u} = (1 - \alpha^2\Delta)^{-1}\mathbf{v}$. For α not zero, using a smoothed velocity $\mathbf{u}$ rather than the original velocity $\mathbf{v}$ suppresses the vortex stretching dynamics, especially for the small scale vortices whose size is less than α.

To give a qualitative idea about how the vortex structures change with increasing α, in Fig. 4 (a-c) we present the iso-surfaces of vorticity for $q/q' = 2$ when $\alpha = 0, 1/32$ and $1/8$, where $q' = \langle q^2 \rangle^{1/2}$ is the *root-mean-square* value of $\mathbf{q}$. It is seen that the tube-like vortex structures [32] persist in all three simulations, implying that the alpha model does not change the qualitative feature of stretching physics. On the other hand, it is evident that with increasing of α, the vortex aspect ratio (characteristic vortex radius/characteristic vortex length) decreases. A similar phenomenon has been noticed in hyperviscosity simulations also [30,31] (where the vortex stretching dynamics is not suppressed) and in subgrid model simulations [29]. However, the physical mechanisms for this phenomena are rather different in the alpha model from the actions of hyperviscosity, since the alpha term affects the nonlinearity (the cause of vortex stretching), while hyperviscosity does not.

One of the most important properties of the vortex stretching dynamics in the Navier-Stokes turbulence is the so-called alignment phenomenon [33], in which the three-dimensional vorticity is locally preferentially aligned with the direction of the second eigenvector of the symmetric strain-rate tensor, $S_{ij} = 1/2(\partial u_i/\partial x_j + \partial u_j/\partial x_i)$. In three-dimensional space, S_{ij} is a 3×3 matrix and has three eigenvalues, λ_1, λ_2 and λ_3. The incompressibility condition leads to:

$$\lambda_1 + \lambda_2 + \lambda_3 = 0.$$

Assume $\lambda_1 \geq \lambda_2 \geq \lambda_3$, then $\lambda_1 \geq 0$ and $\lambda_3 \leq 0$. For the Navier-Stokes turbulence, it has been

found [33] that the spatially averaged λ_2 is greater than zero. Therefore in Navier-Stokes turbulence, the stretching dynamics of vorticity is dominated by two directional expansions with positive eigenvalues and one directional contraction with negative eigenvalue. Since the alpha model is equivalent to filtering the transport velocity in the stretching term for the vorticity equation Eq. (26), it is interesting to study how the alignment phenomenon changes in the alpha model when compared with the Navier-Stokes model.

In Fig. 5 (a-c), we present the probability density functions (PDFs) of the cosine of the angles between the local vorticity and the eigenvectors of the local strain-rate tensor for $\alpha = 0, 1/32$ and $1/8$. The solid lines, the dotted lines and the dotted-dash lines correspond to the maximum eigenvalue, the middle eigenvalue and the minimum eigenvalue, respectively. As expected, the results in Fig. 5(a) (the Navier-Stokes case) are very similar to those results in [33]. The major feature in this plot is that the PDF corresponding to the middle eigenvalue $cos(\theta_2)$ is peaked when $cos(\theta_2) = \pm 1$, implying the alignment mentioned earlier. The PDF of $cos(\theta_3)$ is peaked at the origin, indicating that the vorticity is locally perpendicular to the direction associated with the minimum eigenvalue. The PDF of $cos(\theta_1)$ is almost flat, implying that the direction of vorticity is essentially decorrelated from the direction of the maximum eigenvalue direction. With increasing α, the property of the minimum eigenvalue direction is qualitatively the same, but the PDF of $cos(\theta_1)$ starts forming a peak at ± 1. For $\alpha = 1/8$, the PDF values for $cos(\theta_1)$ at ± 1 are even bigger than those of $cos(\theta_2)$. This result is quite different from the case of the Navier-Stokes equation. We suspect that this new alignment phenomenon (that the vorticity aligns with the direction of the maximum eigenvalue) is connected with the observation (as shown in Fig 4), that the high amplitude vorticity gets thicker as α increases, a result that has also been observed in other subgrid simulations [29].

To further quantify the change of eigenvalues as a function of α, in Fig. 6(a-c), we show the PDFs of the eigenfunctions. There are two essential features in these plots: (i) as α increases, $\langle \lambda_2 \rangle$ keeps positivity, consistent with the result in the Navier-Stokes turbulence; (ii) all eigenvalues tend toward smaller values as α increases, meaning that the stretching is

being suppressed in the alpha model. To study the mean effect of the stretching term on the growth of the enstrophy, $\langle \mathbf{q} \cdot \mathbf{q} \rangle$, in Fig. 7 we present the PDF of $Z \equiv \mathbf{q} \cdot \hat{S} \cdot \mathbf{q}$ as a function of α. The PDFs of these three quantities show very strong intermittency. The flatnesses are $F_{q_i S_{ij} q_j} = 1965$ for $\alpha = 0$, 3566 for $\alpha = 1/32$ and 5319 for $\alpha = 1/8$. The PDFs are strongly positively skewed $(24.28, 35.71$ and $47.02)$ which is consistent with the expectation that the stretching term in the vorticity equation gives a net positive contribution to the dynamics of enstrophy.

V. TWO-POINT STATISTICS

Two-point statistics, primarily the scaling relations of the velocity structure functions in the inertial range, were proposed by Kolmogorov in 1941 [34] based on the self-similarity hypothesis and in 1962 [35] using the idea of the refined similarity hypothesis. Understanding the inertial range intermittent dynamics of fluid turbulence has been a very important focal point for the last few decades, and the two-point inertial range statistics have been extensively examined in experiments at high Reynolds numbers and by numerical simulations at low to moderate Reynolds numbers [31]. In this section, we study the probability density function of the velocity increment and the scalings of the velocity structure functions for systems with various values of α using DNS data, and then compare our measurements with the Kolmogorov theories.

In Fig. 8, we compare the PDFs of the longitudinal velocity gradient, $\partial u/\partial x$, for various alpha values. The derivative here is calculated by a central difference in physical space and a spatial averaging is used for the ensemble averaging in the normalization factor calculation. The main information in this plot is that the PDFs for all three alpha values have close to an exponential tail for large amplitude events. However, the flatnesses of the PDFs (5.0, 4.1 and 3.8 for $\alpha = 0, 1/32$ and $1/8$, respectively) decrease with increasing α. The observed reduction of small scale intermittency is consistent with the energy spectra in Fig. 1 where the high k energy spectra are truncated for large α values. The skewnesses of the PDFs

are $-0.48, -0.51$ and -0.54. In Fig. 9, we present the normalized PDFs of the velocity increment,

$$\Delta_r u \equiv u(x+r) - u(x)$$

in the inertial range when the separation $r = 20$ (in mesh units). It is seen that all three PDFs collapse quite well for most values of $\Delta_r u$, implying that the fundamental features of the two-point statistics in the inertial range do not change much as α varies. This is a very desirable feature in using the alpha model as a subgrid model.

In Fig. 10, we show the second-order structure function, $\langle \Delta_r u \rangle$, versus r at different alpha values. It is seen that when r less than 5 mesh points, the Taylor expansion gives a simple scaling: $\langle \Delta_r u \rangle \sim r^2$. In the narrow inertial range ($20 < r < 60$), the simulation results with $\alpha = 0$ and $1/32$ agree qualitatively with the Kolmogorov $2/3$ scaling [34]. The slightly slower than $2/3$ growth may indicate the intermittent correction. For the case of $\alpha = 1/8$, the filtering of small scale motions significantly decreases the structure function in the inertial range. For this case, the $2/3$ scaling can only been seen for the very narrow region $40 < r < 60$.

In Fig. 11, we present the flatness of the velocity increment, $\langle (\Delta_r u)^4 \rangle / langle (\Delta_r u)^2 \rangle^2$, versus the normalized separation, r/r_0. The normalization length is taken to be half the box length π. As expected, in the small scale region with $r/r_0 < 0.005$, the alpha model is quite different from the Navier Stokes dynamics and the Navier-Stokes equation has the largest flatness value, implying that the Navier-Stokes turbulence is more intermittent than the alpha model dynamics, consistent with the vortex visualization in Fig. 4. It is very interesting to note, however, that the flatnesses versus r/r_0 are almost identical for all three alpha values studied in the narrow inertial range. The decaying of the flatness as a function of r/r_0 implies the existence of an intermittency correction for the scaling exponents. The numerical measurement gives $\langle (\Delta_r u)^4 \rangle / \langle (\Delta_r u)^2 \rangle^2 \sim r^{-0.12}$ in the inertial range. This scaling exponent agrees qualitatively with the value of -0.11 from other direct numerical simulation results [31].

VI. CONCLUDING REMARKS

Our main objective in this paper has been to investigate the utility of the recently proposed alpha equations as a subgrid scale model for three- dimensional turbulence. Our main tool has been direct numerical simulation (DNS) of turbulence in a periodic box. Our conclusions are based on comparisons of DNS using the Navier-Stokes alpha equations for several values of the alpha parameter, including the limiting case $\alpha = 0$ in which the Navier-Stokes equations are recovered. Our principal conclusion is that the alpha model simulations can reproduce most of the large scale features of Navier-Stokes turbulence *even when these simulations do not resolve the fine scale dynamics*, at least in the case of turbulence in a periodic box.

We summarized known analytic properties of the alpha models, including an outline of their derivation and the associated assumptions, their simplification for the case of constant alpha, and their conservation properties. We also offered interpretations of nonlinear dynamics of the alpha models and indicated the changes one might expect from the dynamics of the Navier-Stokes equations.

One of our principal computational results is shown in Fig. 3, where two DNS simulations at $\alpha = 1/8$, but using two different resolutions, are compared with each other and with a Navier-Stokes simulation (representing truth). The spectra are identical for the larger wavelengths, demonstrating (in this case) that one does not need to resolve the small scale dynamics to reproduce the large scale features of the turbulence.

We further compared vorticity structures and alignment, and also two point statistics to illustrate the altered dynamics of the alpha models. In general, we found consistency of these DNS results with our expectations based on analysis.

The use of the alpha equations as a subgrid model of turbulent flows in more complicated geometries and forcings remains to be studied. However we believe these first results are very promising.

VII. ACKNOWLEDGMENTS

We thank C. Foias, R. H. Kraichnan, J. C. McWilliam, E. Olson, K. R. Sreenivasan, E.S. Titi and S. Wynne, for helpful discussions. Numerical simulations were carried out at the Advanced Computing Laboratory at Los Alamos National Laboratory using the SGI machines. We appreciate the support and computer time provided by the US Department of Energy Climate Change Prediction Program.

REFERENCES

[1] D.D. Holm, J.E. Marsden, T.S. Ratiu, Adv. in Math. **137** (1998) 1.

[2] D.D. Holm, J.E. Marsden, T.S. Ratiu, Phys. Rev. Lett. **80** (1998) 4173.

[3] R. Camassa and D.D. Holm, Phys. Rev. Lett. **71** (1993) 1661.

[4] D.D. Holm, S. Kouranbaeva, J.E. Marsden, T. Ratiu and S. Shkoller, *Fields Inst. Comm., Arnold Vol. 2*, Amer. Math. Soc., (Rhode Island) (1998) to appear.

[5] D.D. Holm, Physica D, to appear.

[6] S. Chen, C. Foias, D.D. Holm, E. Olson, E.S. Titi, S. Wynne, Phys. Rev. Lett., **81** (1998) 5338.

[7] S. Chen, C. Foias, D.D. Holm, E. Olson, E.S. Titi, S. Wynne, Phys. Fluids, to appear.

[8] S. Chen, C. Foias, D.D. Holm, E. Olson, E.S. Titi, S. Wynne, Physica D, to appear.

[9] M.V. Zagarola, Ph.D thesis, Princeton University (1996).

[10] C. Foias, D.D. Holm and E.S. Titi, *The 3D viscous Camassa–Holm equations: their relation to the Navier–Stokes equations and turbulence Theory*, in preparation.

[11] J.E. Dunn and R.L. Fosdick, Arch. Rat. Mech. Anal., **56** 191 (1974).

[12] D. Cioranescu and V. Girault, C. R. Acad. Sc. Paris Série 1, **322** (1996) 1163.

[13] D. Cioranescu and V. Girault, Int. J. Non-Lin. Mech. **32** (1997) 317.

[14] D.G. Andrews and M.E. McIntyre, J. Fluid Mech. **89** (1978) 609.

[15] J.E. Dunn and R.L. Fosdick, Arch. Rat. Mech. Anal. **56** (1974) 191.

[16] J.E. Dunn and K.R. Rajagopal, Int. J. Engng. Sci. **33** (1995) 689.

[17] R. S. Rivlin, Q. Appl. Math. **15** (1957) 212.

[18] A. J. Chorin, Phys. Rev. Lett. **60** (1988) 1947.

[19] T.H. Shih, J. Zhu and J.L. Lumley, Comput. Methods Appl. Mech. Engng. **125** (1995) 287.

[20] A. Yoshizawa, Phys. Fluids, **27** (1984) 1377.

[21] R. Rubinstein and J.M. Barton, Phys. Fluids A, **2** (1990) 1472.

[22] J.O. Hinze, *Turbulence*, (Mc-Graw-Hill: New York, 2nd edition, 1975).

[23] A.A. Townsend, *The Structure of Turbulent Flows*, (Cambridge University Press, 1967).

[24] J.L. Lumley and H. Tennekes, *A First Course in Turbulence*, (MIT Press, 1972).

[25] W. C. Reynolds, Fundamentals of turbulence for turbulence modeling and simulation, in: *Lecture Notes for Von Karman Institute*, AGARD Lecture Note Series, (NATO, New York, 1987) pp.1-66.

[26] U. Piomelli, Applications of large eddy simulations in engineering: an overview, in: *Large-eddy Simulation of Complex Engineering and Geophysical Flows*, ed. B. Galperin and S. A. Orszag (Cambridge University Press, 1993).

[27] M. Lesieur and O. Métais, Annual Rev. Fluid Mech. **28** (1996) 45.

[28] S. Y. Chen and X. Shan, Comput. Phys. **6** (1992) 643.

[29] Lian-Ping Wang, Shiyi Chen, James G. Brasseur and John C. Wyngaard, " J. Fluid Mechanics, **309** (1996) 113.

[30] V. Borue and S. A. Orszag, Europhy. Lett. **29** (1995) 687.

[31] N. Cao, S. Chen and Z. She, Phys. Rev. Lett., **76** (1996) 3711.

[32] N. Cao, S. Chen and G. D. Doolen, *Statistics and Structures of Pressure in Isotropic Turbulence*, Physics of Fluids, in press (1999).

[33] W. T. Ashurst, A. R. Kerstein, R. M. Kerr and C. H. Gibson, Phys. Fluids, **30** (1987) 2343.

[34] A.N. Kolmogorov, "The local structure of turbulence in incompressible viscous fluid for very large Reynolds numbers," Dokl. Adad. Nauk SSSR **30**, 301 (1941).

[35] A.N. Kolmogorov, "A refinement of previous hypotheses concerning the local structure of turbulence in a viscous incompressible fluid at high Reynolds number," J. Fluid Mech. **13**, 82 (1962).

VIII. FIGURE CAPTIONS

Fig. 1. The energy spectrum, $E(k)$, versus the wave number k for $\alpha = 0$ (solid line), 1/32 (dotted line) and 1/8 (dotted-dash line). In the inertial range ($k < 10$), a power spectrum with $k^{-5/3}$ can be identified.

Fig. 2. Energy spectra for $\alpha = 1/8$ with 256^3 (dotted line) and 64^3 (dashed-dot line), and compared with the Navier-Stokes simulation (the solid line).

Fig. 3. The energy transfer spectrum, $\Pi(k)$ versus k for $\alpha = 0$ (solid line), 1/32 (dotted line) and 1/8 (dotted-dash line).

Fig. 4. Three-dimensional view of vorticity iso-surfaces for $\alpha = 0$ (a), 1/32 (b) and 1/8 (c) when $q/q' = 2$, where q' is the *rms* of the vorticity. The data are from 256^3 simulations and only one eighth of the simulation domain is shown.

Fig. 5. The probability density function of $cos(\theta)$ for simulations with $\alpha = 0$ (a), 1/32 (b) and 1/8 (c). In each plot, the solid line, the dotted line and the dotted-dash line are for the maximum, middle and minimum eigenvalue, respectively.

Fig. 6. The probability density functions for the maximum eigenvalue λ_1 (a), the middle eigenvalue λ_2 (b) and the minimum eigenvalue λ_3 (c). The solid line, the dotted line and the dotted-dash line are for $\alpha = 0, 1/32$ and 1/8, respectively.

Fig. 7. Normalized PDFs of $z = q_i S_{ij} q_j$ for $\alpha = 0$ (solid line), 1/32 (dotted line) and 1/8 (dotted-dash line).

Fig. 8. Normalized PDFs of the longitudinal velocity gradient, $\partial u/\partial x$ for $\alpha = 0$ (solid line), 1/32 (dotted line) and 1/8 (dotted-dash line).

Fig. 9. Normalized PDFs of the velocity increment in the inertial range for $\alpha = 0$ (solid line), 1/32 (dotted line) and 1/8 (dotted-dash line).

Fig. 10. The second order structure function as a function of r for $\alpha = 0$ (solid line), 1/32 (dotted line) and 1/8 (dotted-dash line). The dashed line is the scaling prediction by Kolmogorov [34].

Fig. 11. The flatness, $\langle(\Delta_r u)^4\rangle/\langle(\Delta_r u)^2\rangle^2$, as a function of separation r/r_0 for $\alpha = 0$ (solid line), 1/32 (dotted line) and 1/8 (dotted-dash line). Here r_0 is taken as half the box size, π.

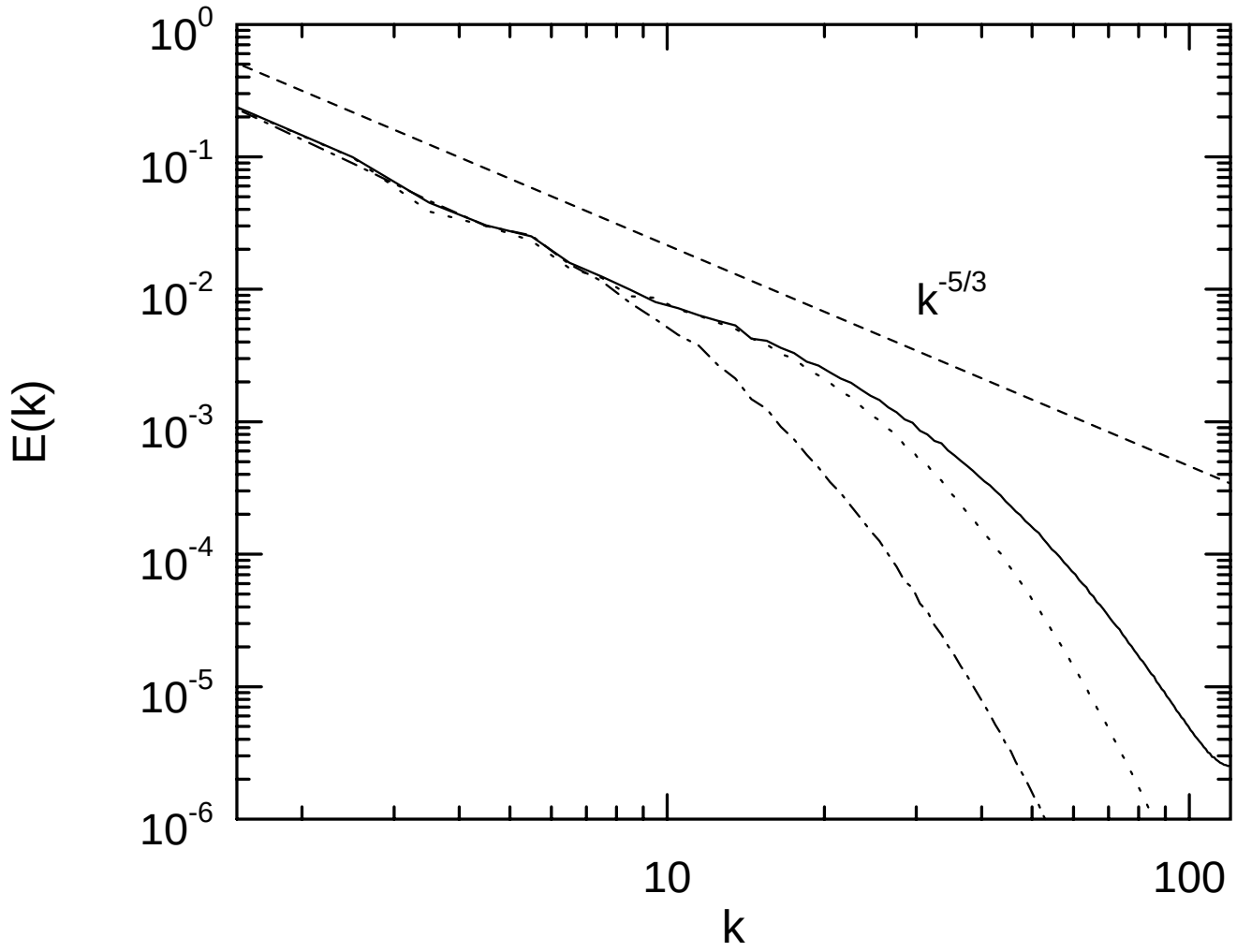
E(k)
10^{0}
10^{-1}
10^{-2}
10^{-3}
10^{-4}
10^{-5}
10^{-6}
$k^{-5/3}$
10
100
k

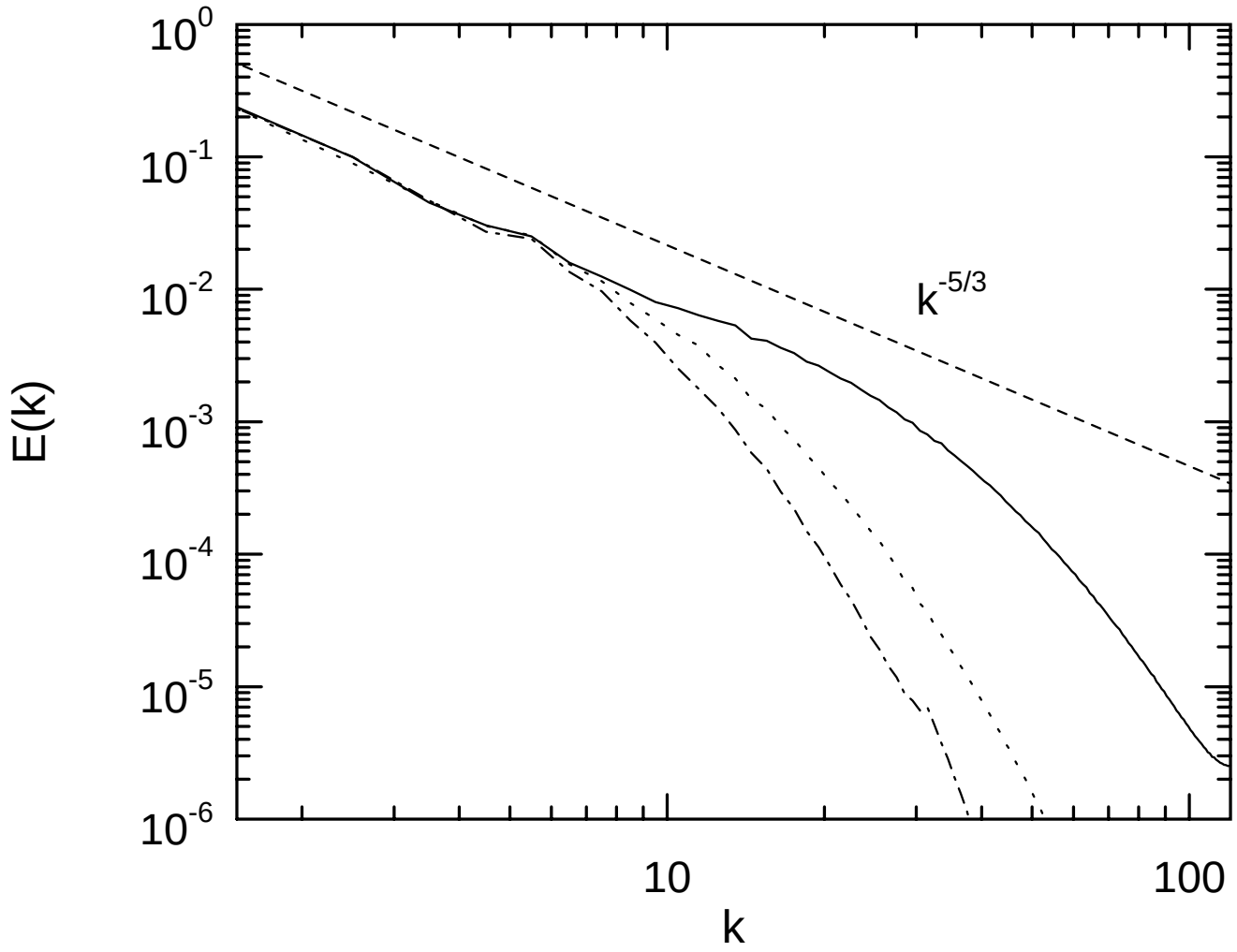
10^0
10^{-1}
10^{-2}
10^{-3}
10^{-4}
10^{-5}
10^{-6}
E(k)
$k^{-5/3}$
10
100
k

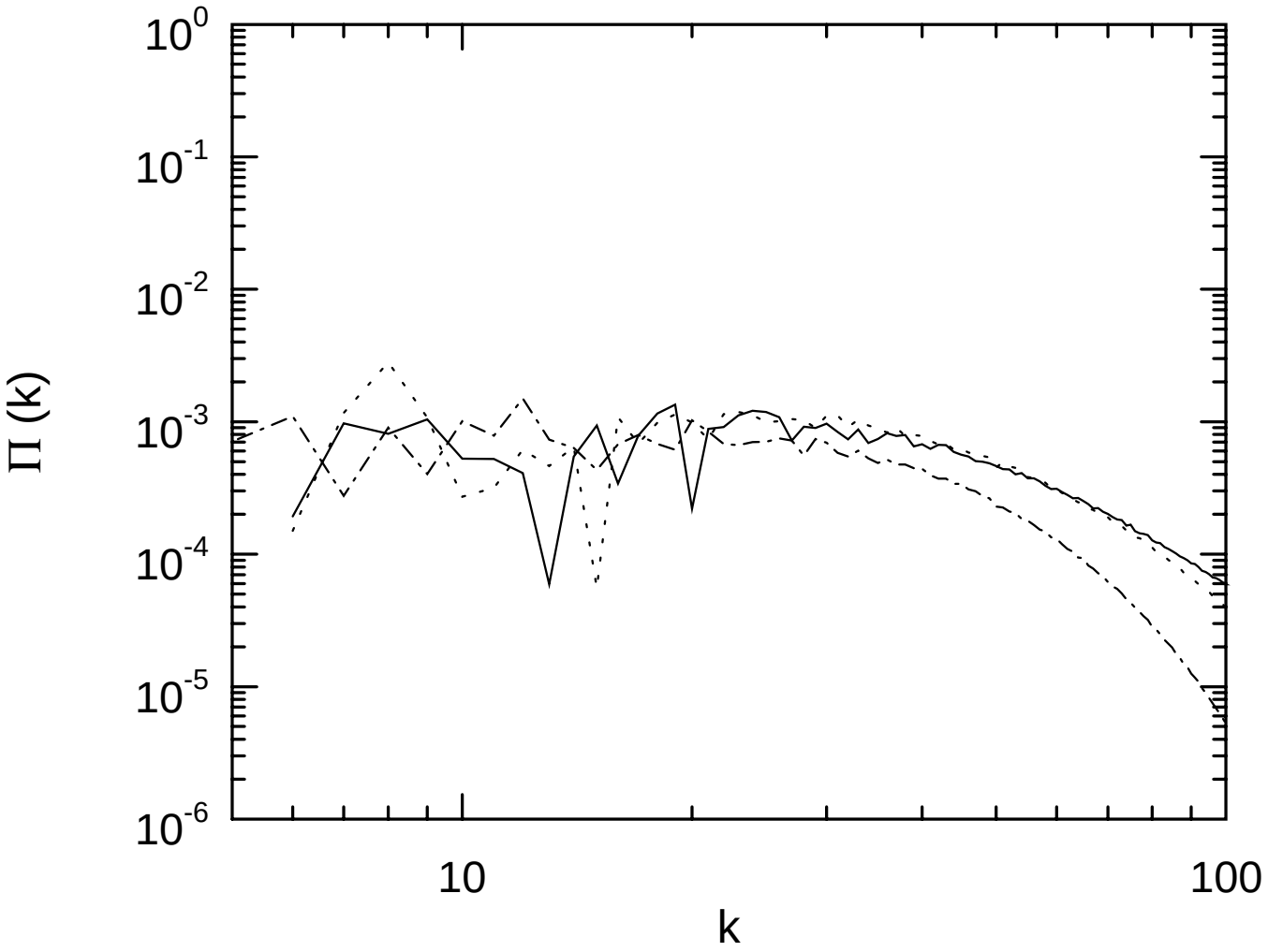
10^0
10^{-1}
10^{-2}
10^{-3}
10^{-4}
10^{-5}
10^{-6}
Π (k)
10
100
k

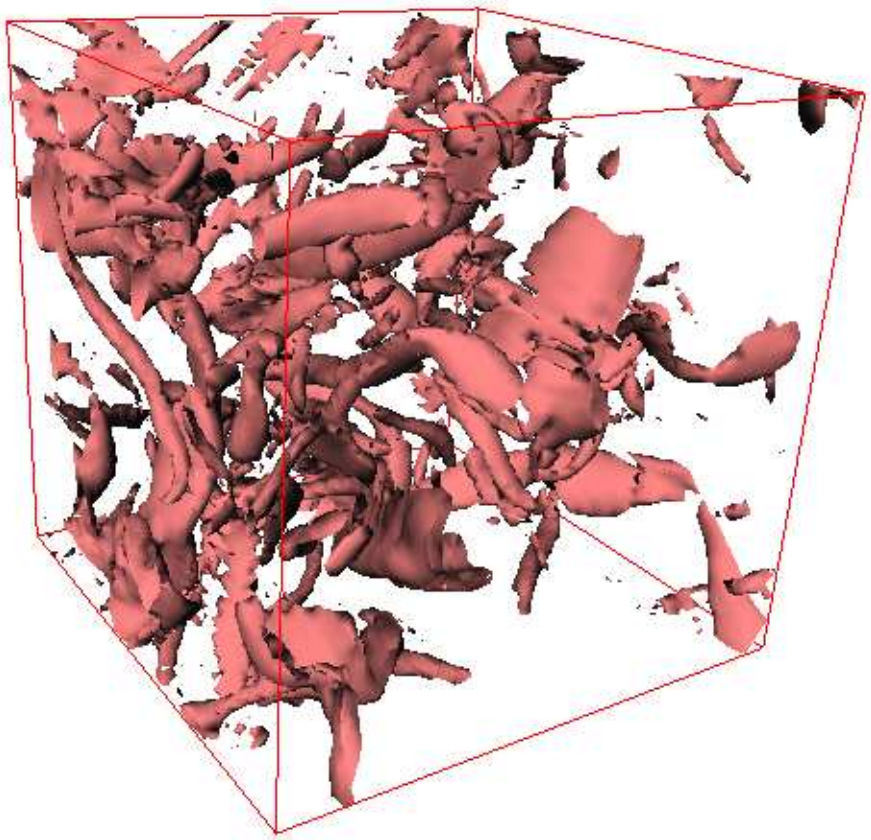

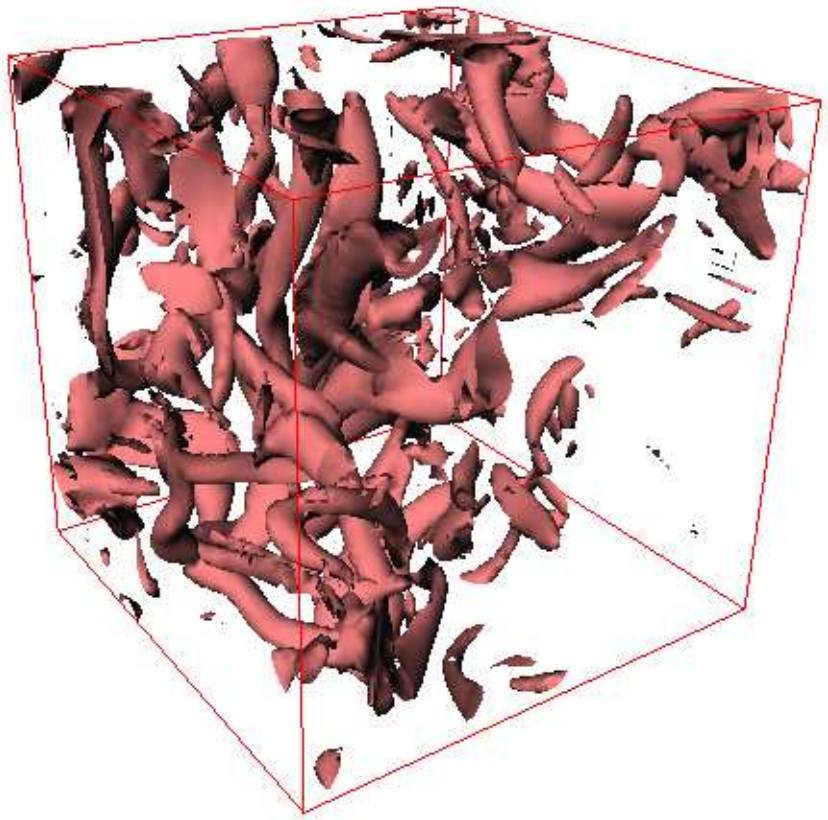

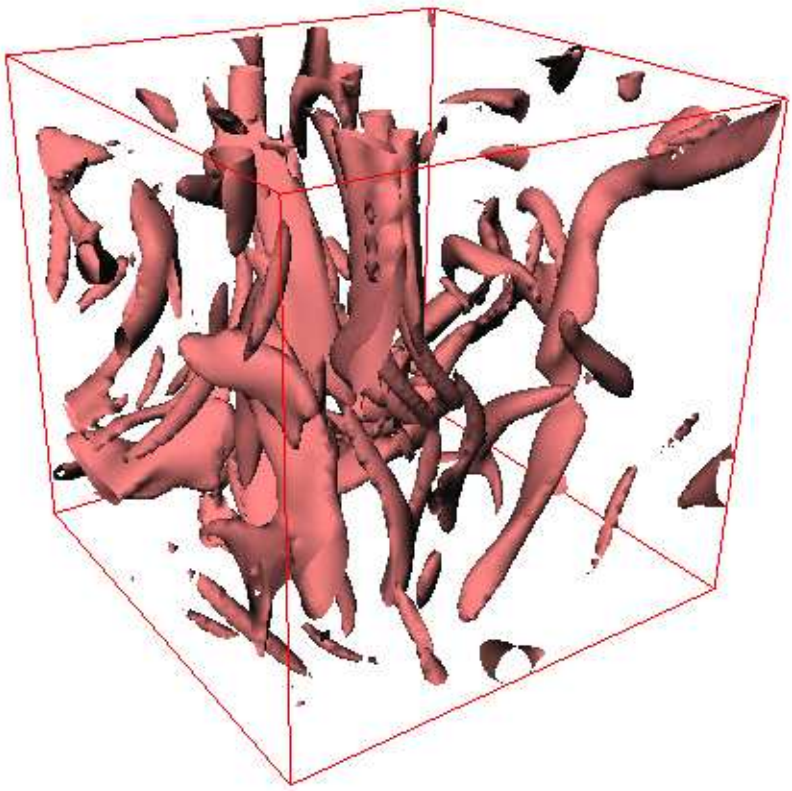

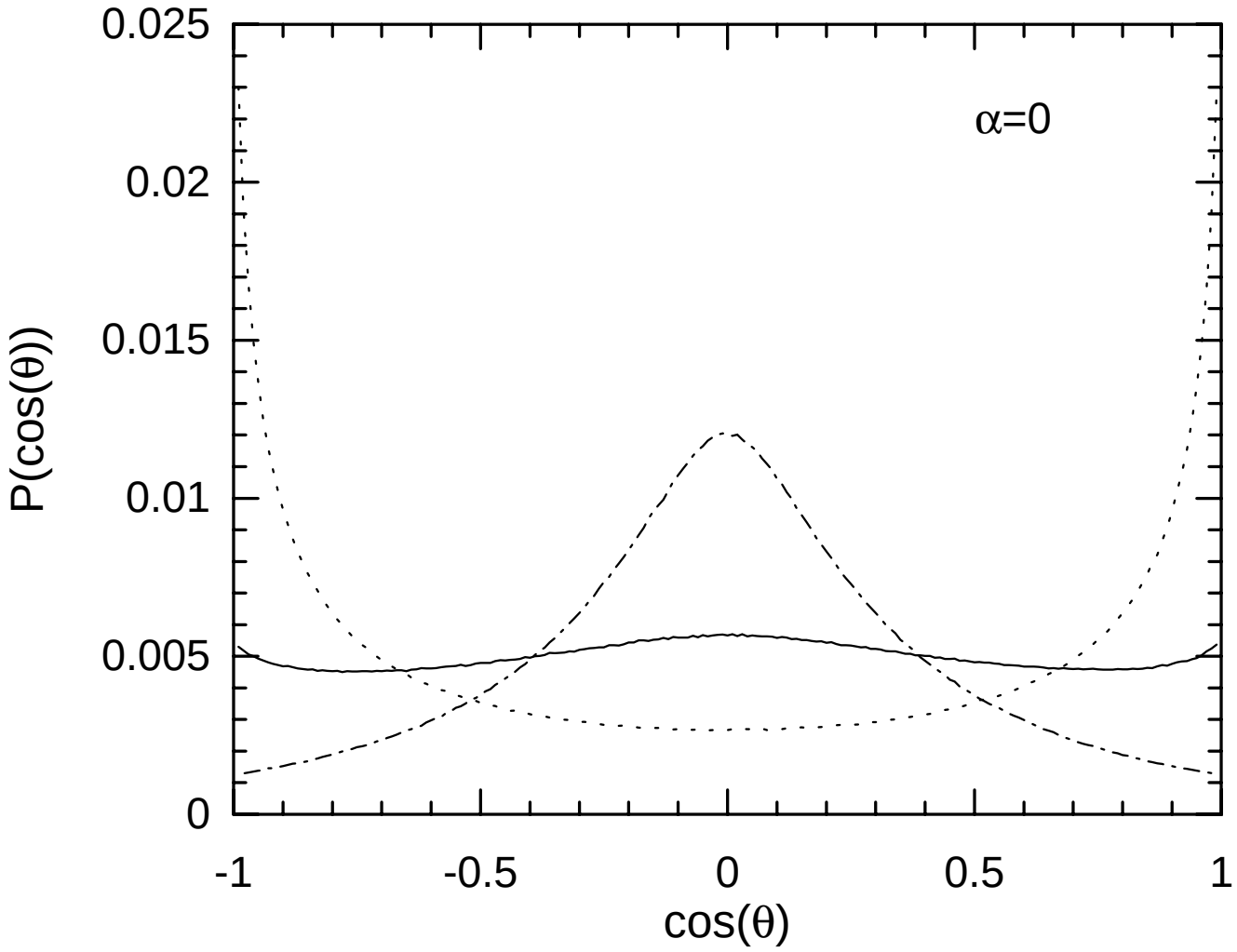
0.025
0.02
0.015
0.01
0.005
0
P(cos(θ))
α=0
-1
-0.5
0
0.5
1
cos(θ)

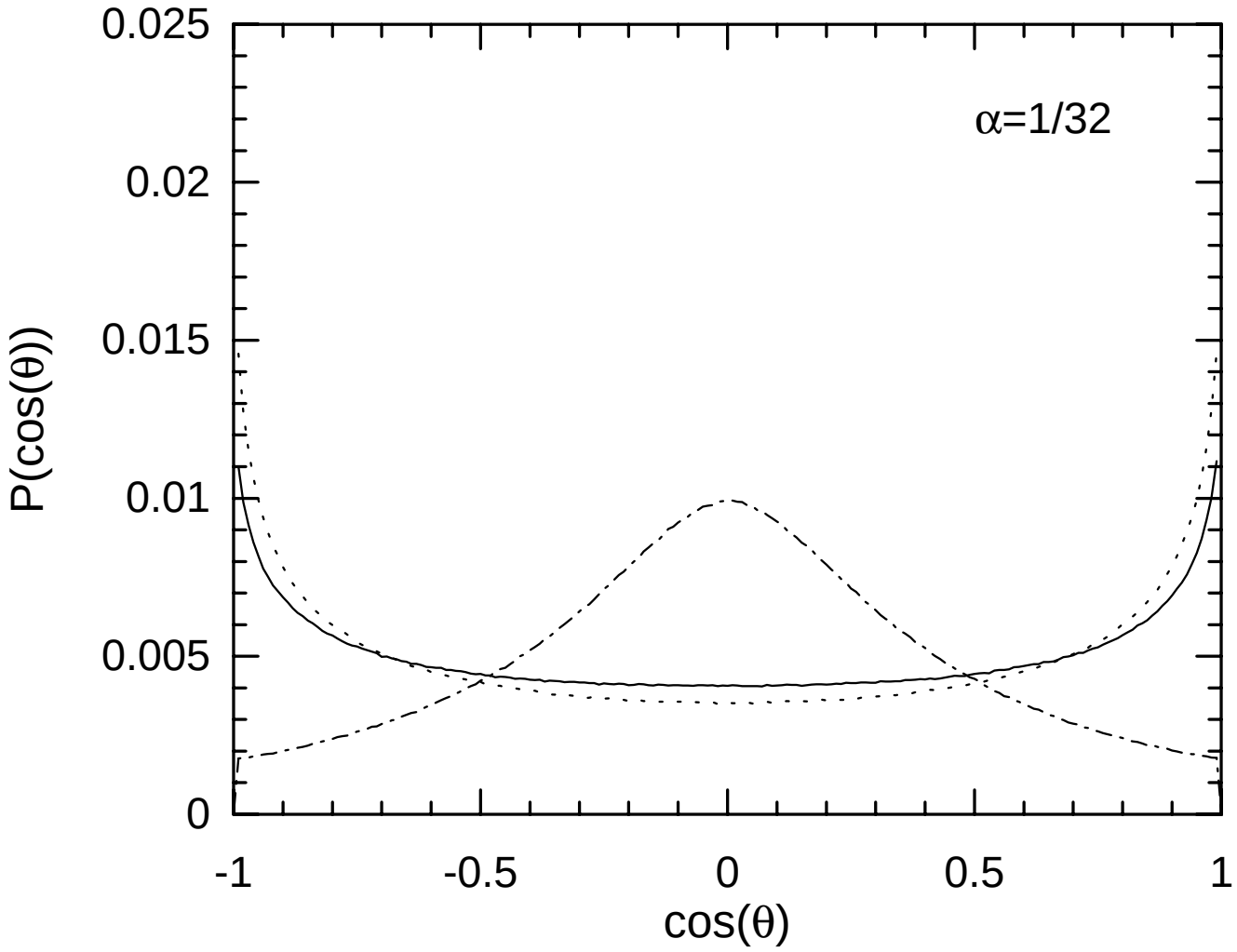
0.025
0.02
0.015
0.01
0.005
0
P(cos(θ))
α=1/32
-1
-0.5
0
0.5
1
cos(θ)

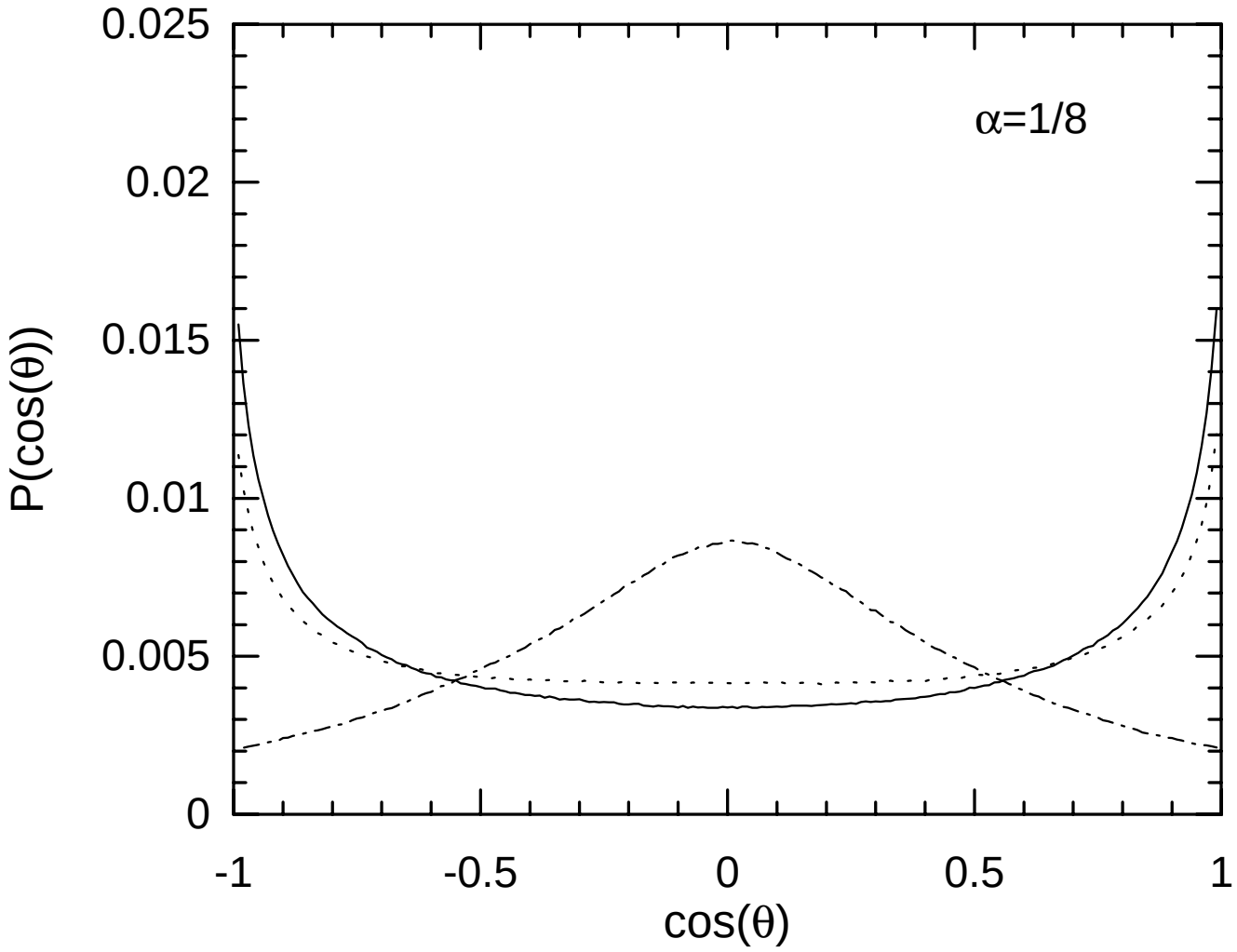
0.025
0.02
0.015
0.01
0.005
0
P(cos(θ))
α=1/8
-1
-0.5
0
0.5
1
cos(θ)

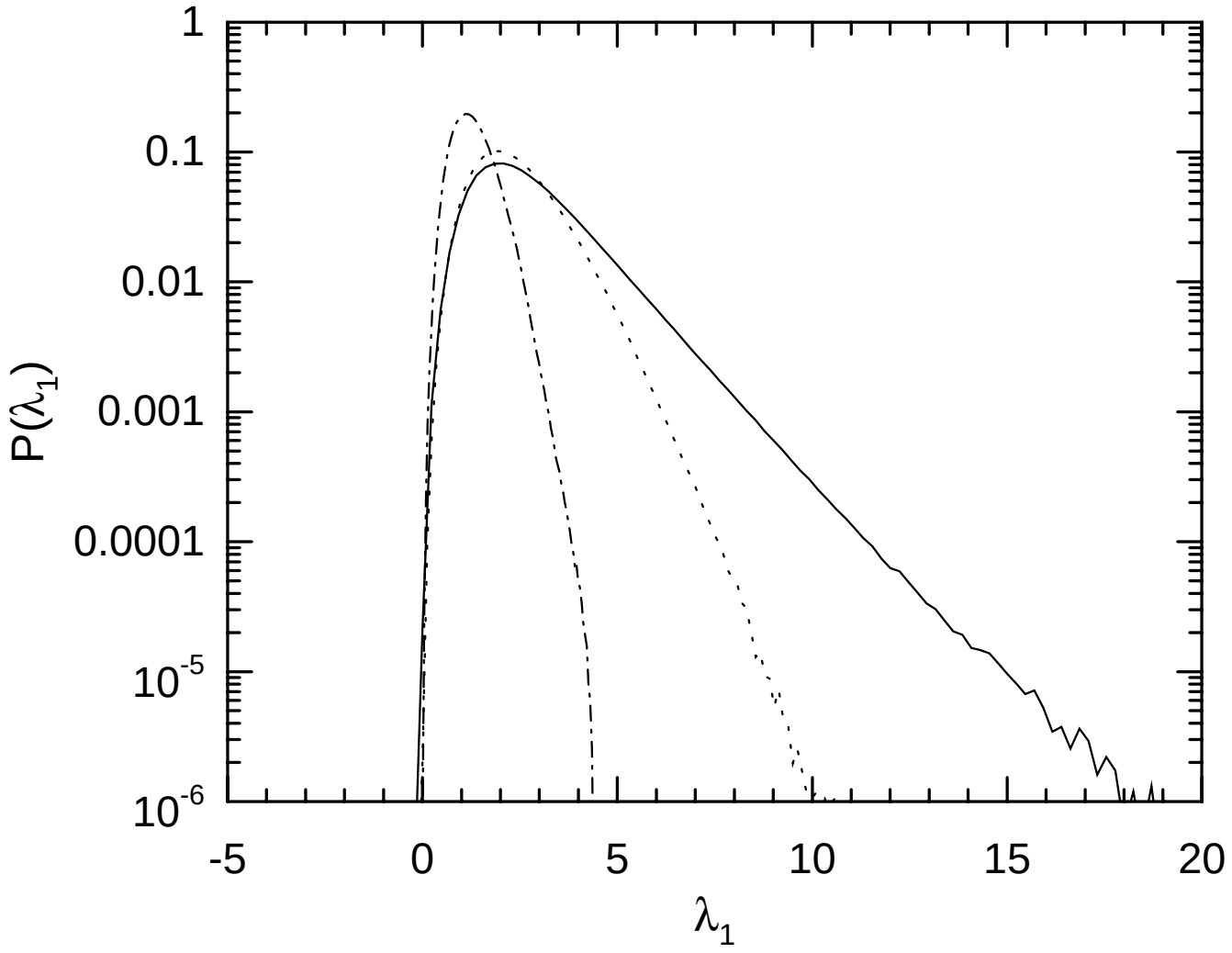
1
0.1
0.01
0.001
0.0001
10^-5
10^-6
P(λ1)
-5
0
5
10
15
20
λ1

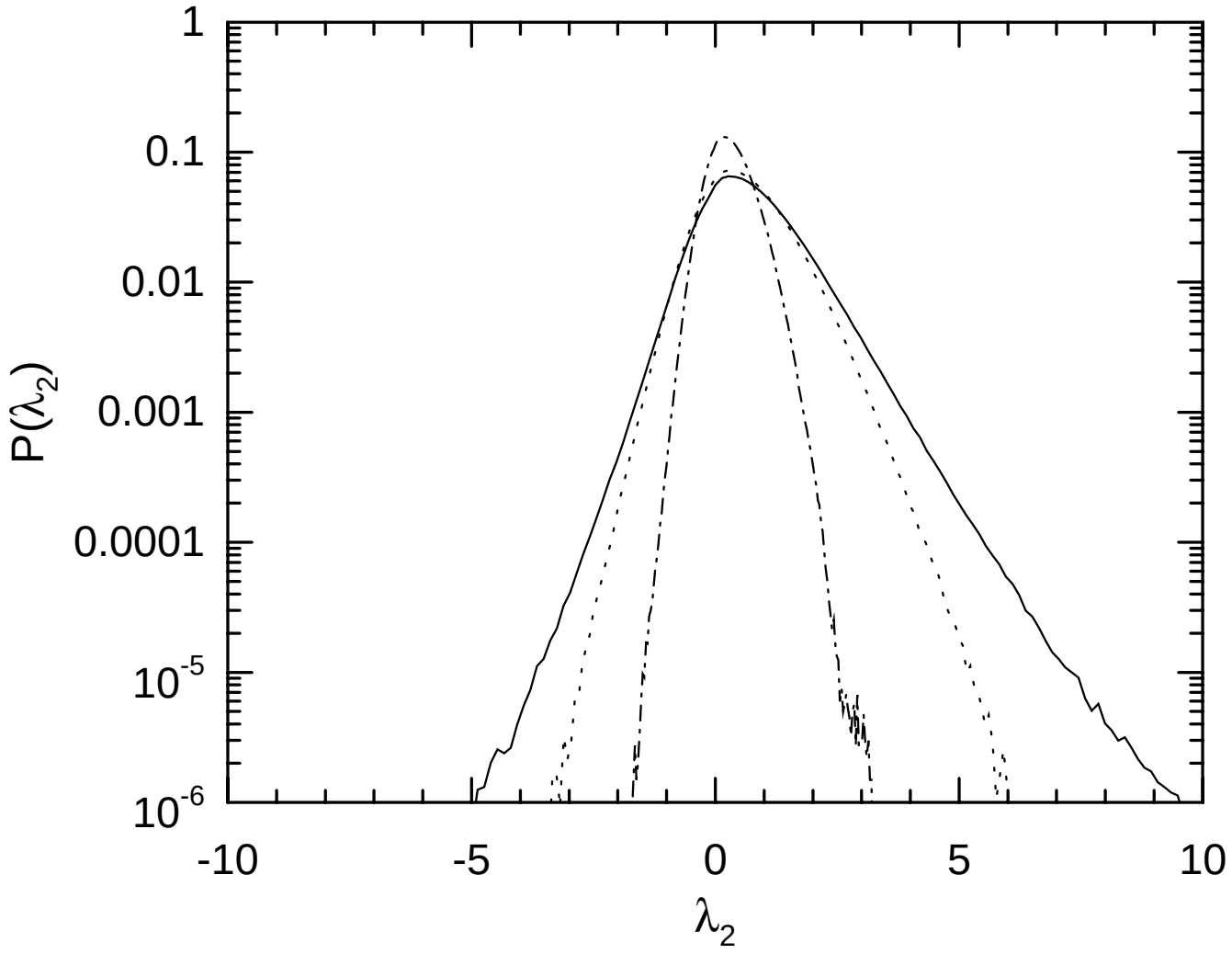
1
0.1
0.01
0.001
0.0001
10-5
10-6
P(λ2)
-10
-5
0
5
10
λ2

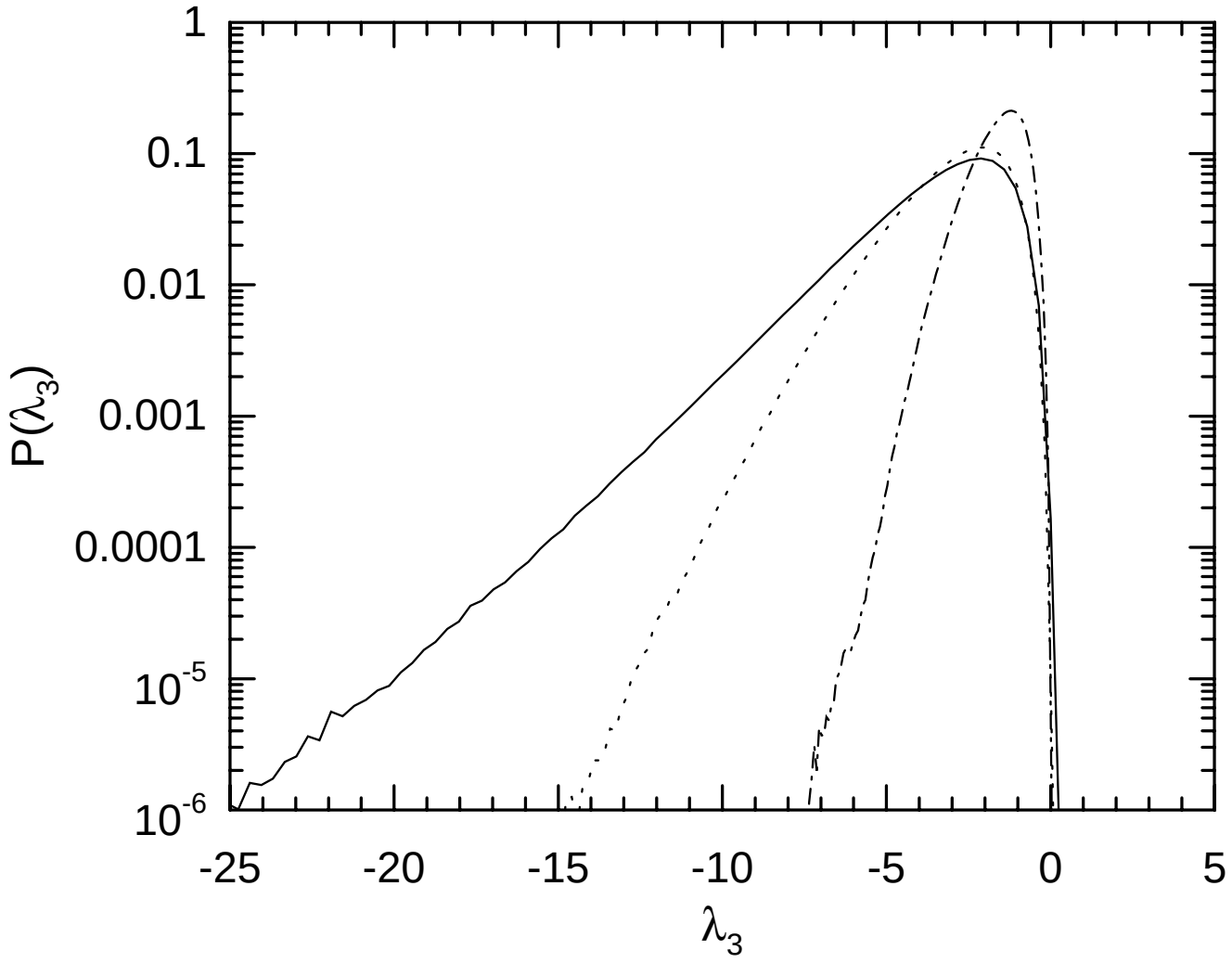
1
0.1
0.01
0.001
0.0001
10^-5
10^-6
P(λ3)
-25
-20
-15
-10
-5
0
5
λ3

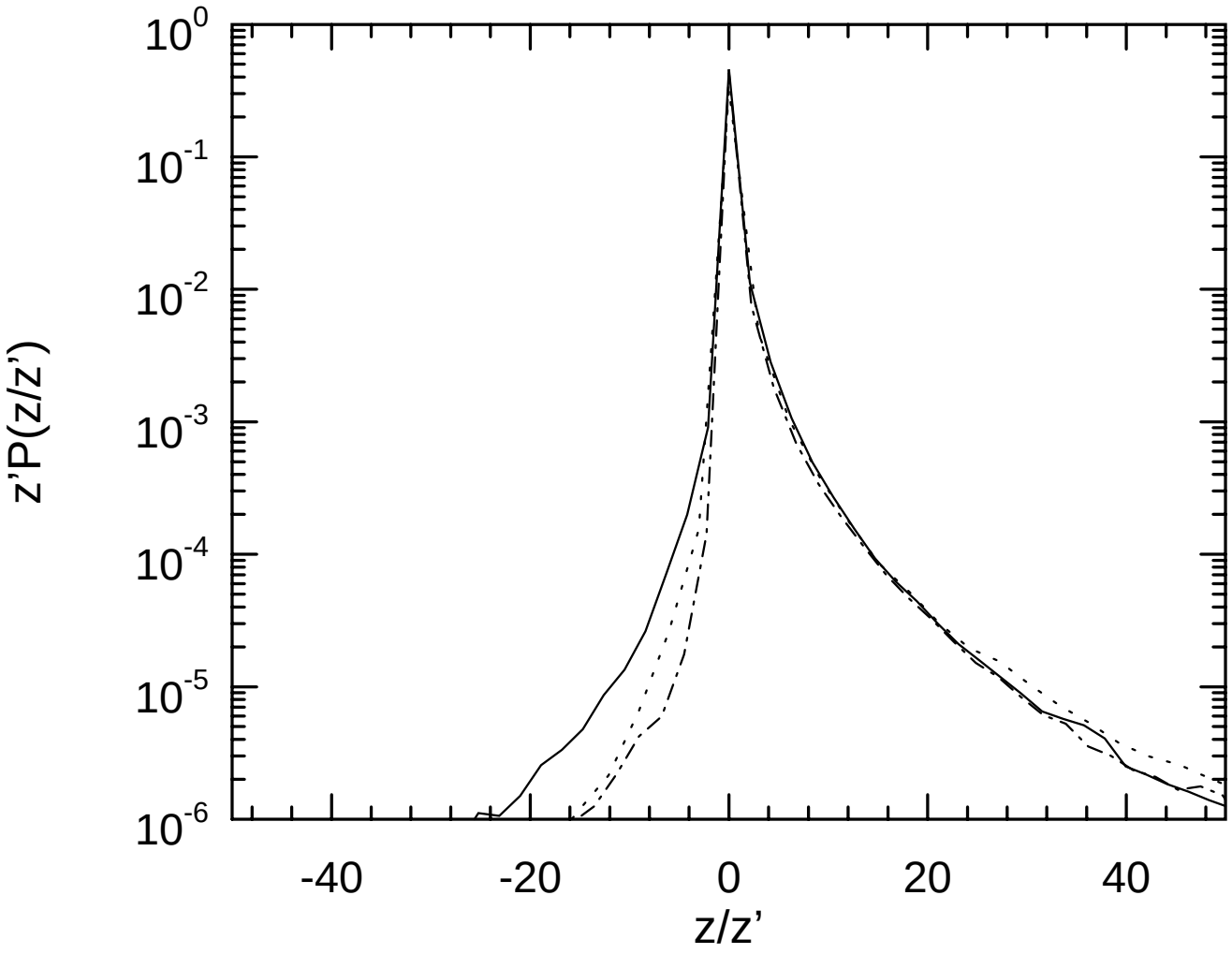
10^0
10^{-1}
10^{-2}
10^{-3}
10^{-4}
10^{-5}
10^{-6}
z'P(z/z')
-40
-20
0
20
40
z/z'

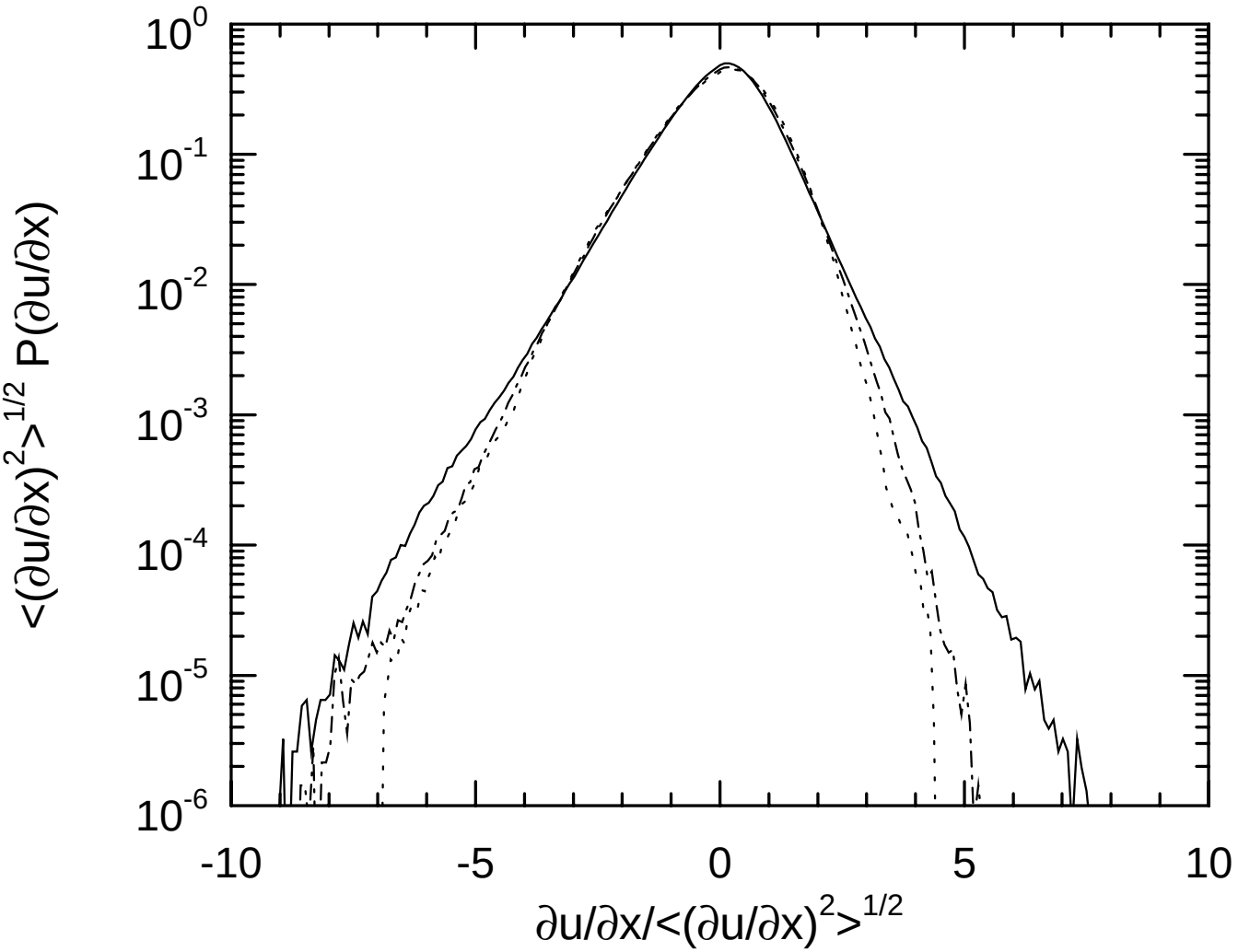
10^0
10^{-1}
10^{-2}
10^{-3}
10^{-4}
10^{-5}
10^{-6}
-10
-5
0
5
10
$<(\partial u/\partial x)^2>^{1/2}$ P($\partial u/\partial x$)
$\partial u/\partial x/<(\partial u/\partial x)^2>^{1/2}$

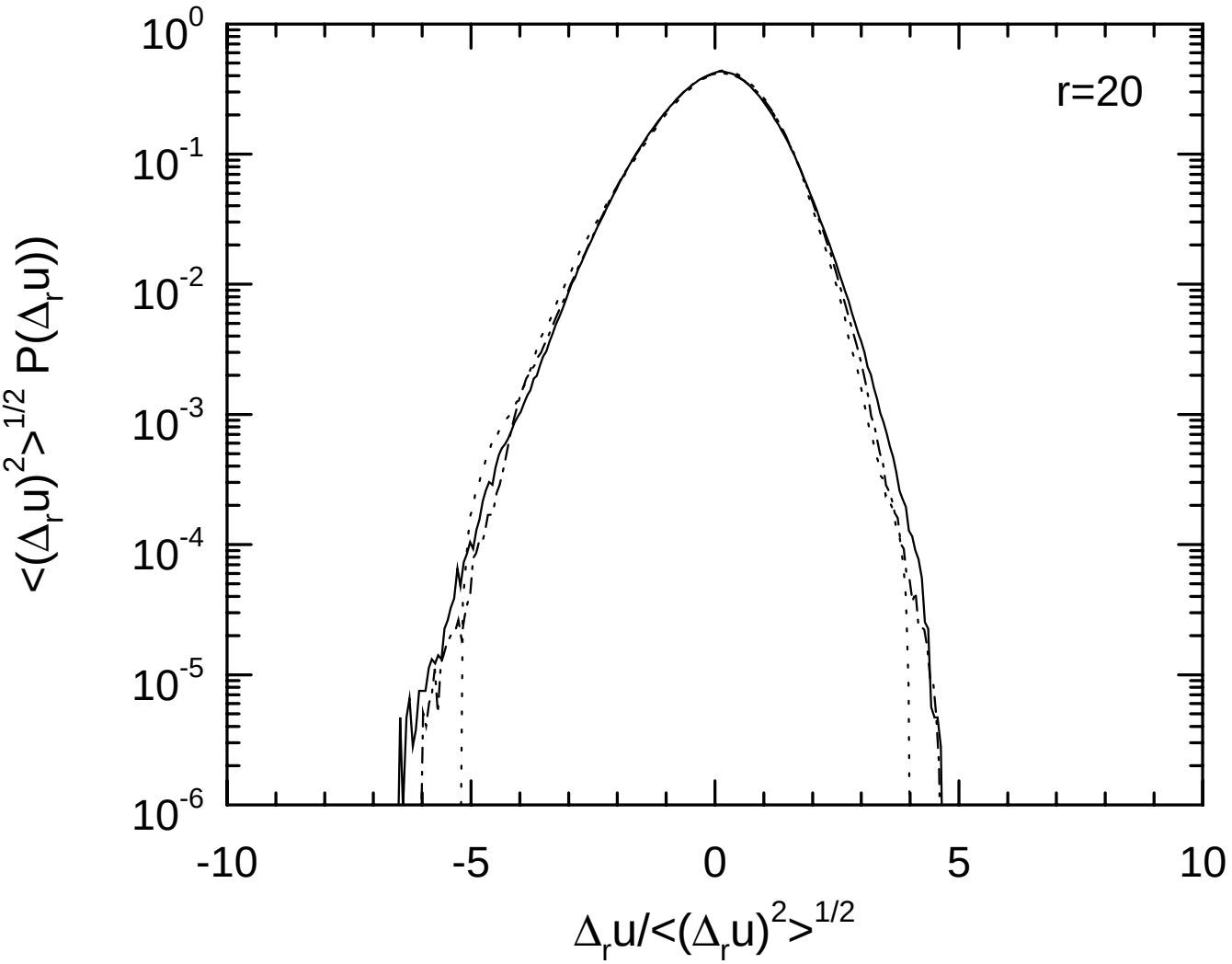
r=20
10^0
10^{-1}
10^{-2}
10^{-3}
10^{-4}
10^{-5}
10^{-6}
-10
-5
0
5
10
$<(\Delta_r u)^2>^{1/2} P(\Delta_r u))$
$\Delta_r u/<(\Delta_r u)^2>^{1/2}$

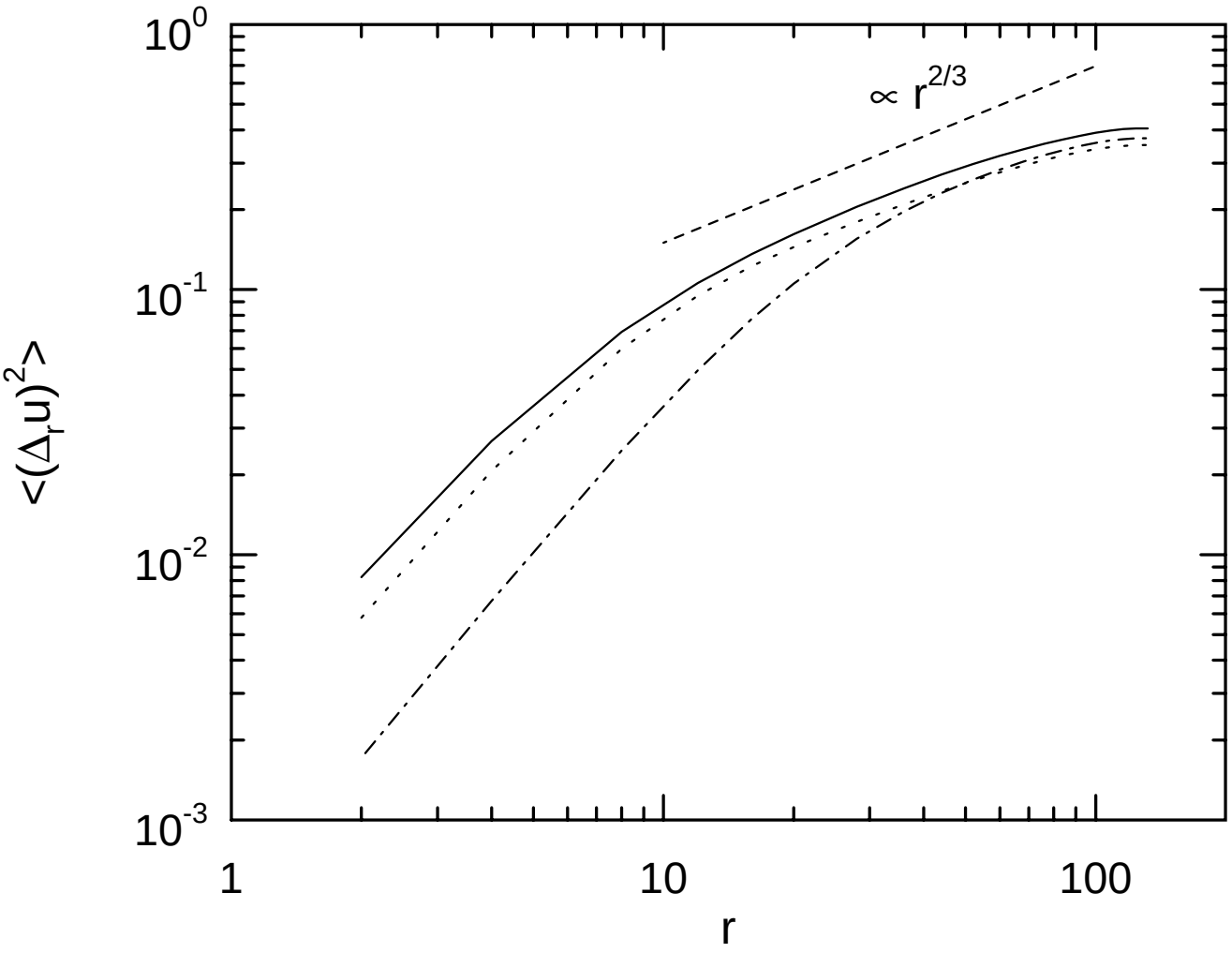
10^0
10^{-1}
10^{-2}
10^{-3}
$\propto r^{2/3}$
$<(\Delta_r u)^2>$
1
10
100
r

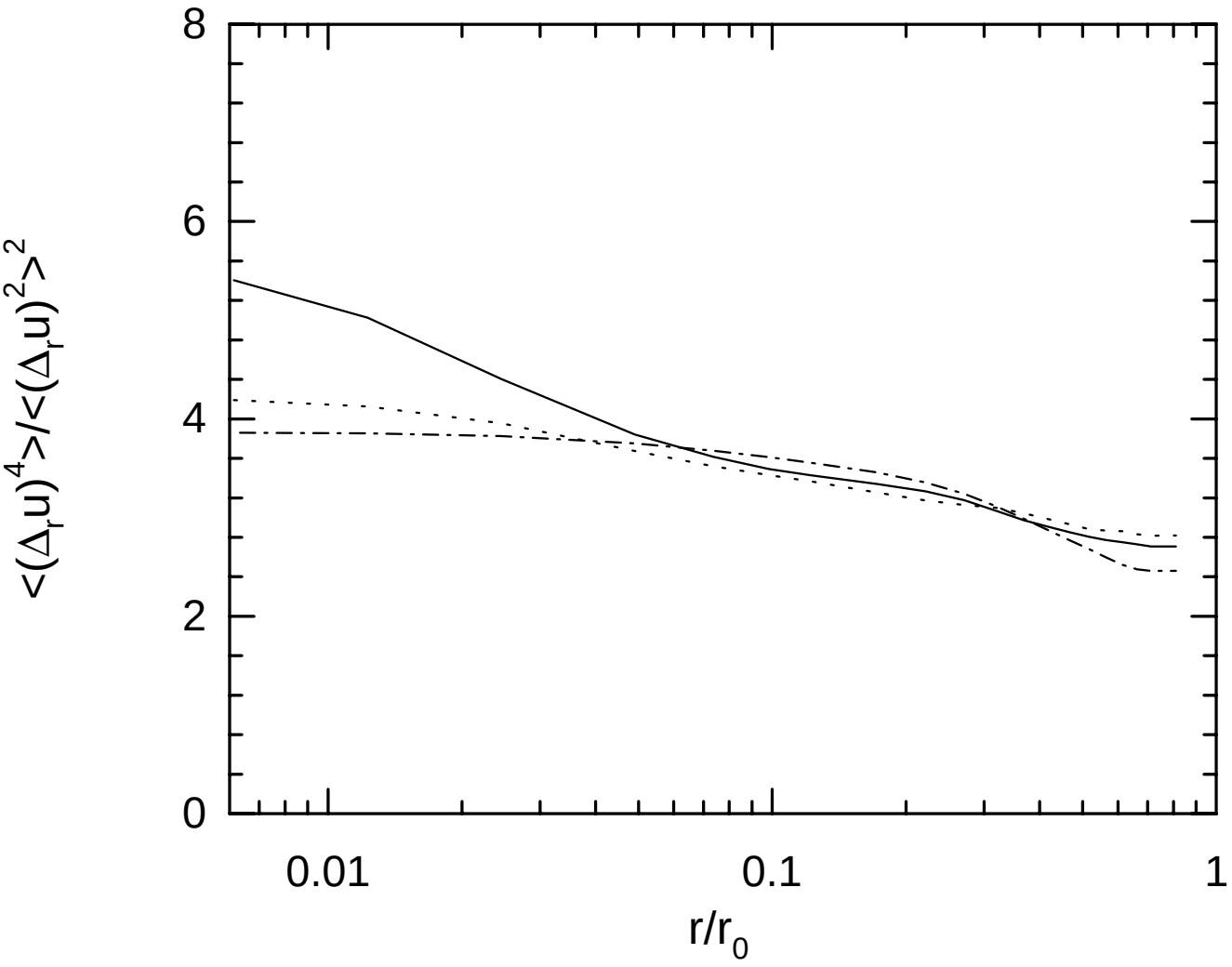
8
6
4
2
0
0.01
0.1
1
r/r0
<(Δru)4>/<(Δru)2>2